Article

Developmental Cell

Distinct epicardial gene regulatory programs drive development and regeneration of the zebrafish heart

Graphical abstract

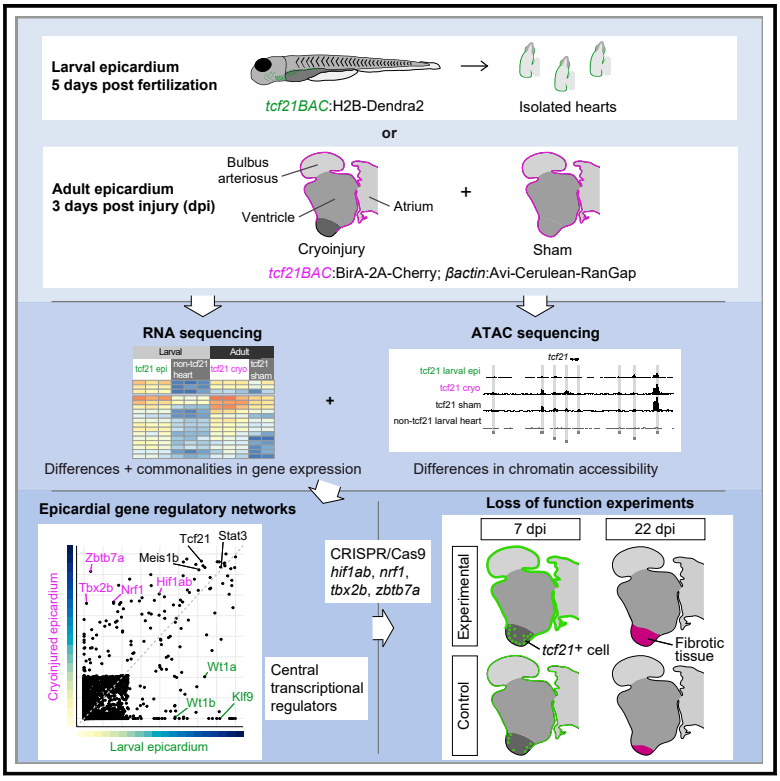

Highlights

- Epicardial gene expression in regenerating and developing zebrafish heart is distinct
- Epicardial chromatin accessibility differs between heart regeneration and development
- Hif1ab, Nrf1, Tbx2b, and Zbtb7a are key regulators of the regenerating epicardium
- Loss of Hif1ab, Nrf1, Tbx2b, and Zbtb7a increases *tcf21*$^{+}$ cell numbers following injury

Authors

Michael Weinberger, Filipa C. Simões, Trishalee Gungoosingh, Tatjana Sauka-Spengler, Paul R. Riley

Correspondence

TSauka-Spengler@stowers.org (T.S.-S.), paul.riley@idrm.ox.ac.uk (P.R.R.)

In brief

Weinberger and Simões et al. detail transcriptomic and epigenomic differences between regenerating adult and developing larval zebrafish epicardium. Constructing gene regulatory networks, they identify transcription factors regulating each setting, with loss of adult epicardial regulators Hif1ab, Nrf1, Tbx2b, and Zbtb7a increasing epicardial cell numbers following injury and affecting heart regeneration.

Weinberger et al., 2024, Developmental Cell *59*, 351–367
February 5, 2024
https://doi.org/10.1016/j.devcel.2023.12.012

CellPress

Developmental Cell

CellPress
OPEN ACCESS

Article

Distinct epicardial gene regulatory programs drive development and regeneration of the zebrafish heart

Michael Weinberger,[1,2,4] Filipa C. Simões,[1,4] Trishalee Gungoosingh,[1] Tatjana Sauka-Spengler,[2,3,5,*] and Paul R. Riley[1,5,6,*]

[1]Department of Physiology, Anatomy and Genetics, Institute of Developmental & Regenerative Medicine, University of Oxford, Oxford OX3 7TY, Oxfordshire, UK
[2]Radcliffe Department of Medicine, MRC Weatherall Institute of Molecular Medicine, University of Oxford, Oxford OX3 9DS, Oxfordshire, UK
[3]Stowers Institute for Medical Research, Kansas City, MO, USA
[4]These authors contributed equally
[5]Senior author
[6]Lead contact
*Correspondence: TSauka-Spengler@stowers.org (T.S.-S.), paul.riley@idrm.ox.ac.uk (P.R.R.)
https://doi.org/10.1016/j.devcel.2023.12.012

SUMMARY

Unlike the adult mammalian heart, which has limited regenerative capacity, the zebrafish heart fully regenerates following injury. Reactivation of cardiac developmental programs is considered key to successfully regenerating the heart, yet the regulation underlying the response to injury remains elusive. Here, we compared the transcriptome and epigenome of the developing and regenerating zebrafish epicardia. We identified epicardial enhancer elements with specific activity during development or during adult heart regeneration. By generating gene regulatory networks associated with epicardial development and regeneration, we inferred genetic programs driving each of these processes, which were largely distinct. Loss of Hif1ab, Nrf1, Tbx2b, and Zbtb7a, central regulators of the regenerating epicardial network, in injured hearts resulted in elevated epicardial cell numbers infiltrating the wound and excess fibrosis after cryoinjury. Our work identifies differences between the regulatory blueprint deployed during epicardial development and regeneration, underlining that heart regeneration goes beyond the reactivation of developmental programs.

INTRODUCTION

In mammals, the capacity to repair the heart following injury rapidly declines after birth.[1,2] In contrast, the zebrafish heart can regenerate throughout adulthood,[3–6] offering the possibility to investigate the mechanisms underlying cardiac regeneration.[7,8] The epicardium, a mesothelial layer of cells enveloping the vertebrate heart muscle, is essential for heart development[9] and critically required for zebrafish heart regeneration.[10] While epicardial cells in the homeostatic adult heart are mostly dormant, they become activated following cardiac injury. Activated epicardial cells re-enter the cell cycle and re-express developmental genes such as the transcription factors (TFs) *tbx18* and *wt1b*.[3,11–14] Initially, epicardial cell activation is an organ-wide response fully manifested by 3 days post-injury (dpi) and then becomes restricted to the site of injury by 7 dpi.[3,14] Activated epicardial cells are among the first to migrate into the injury area, depositing extracellular matrix (ECM) components such as fibronectin and collagens.[15–17] The activated epicardium further acts as a major signaling hub,[13,18–22] and epicardium-derived cells (EPDCs) invade the subepicardial tissue,[9] giving rise to perivascular cells and fibroblasts.[11] Thus, the epicardium supports heart regeneration both directly and indirectly.

Across species, recapitulation of developmental programs has generally been considered a key feature to successfully regenerate the heart following injury.[23–25] In the epicardium, many of the factors expressed by activated adult cells are also expressed by the developing epicardium, and epicardial functions during heart regeneration and development are very similar.[9] However, it has previously been demonstrated that expression profiles of selected cell-surface markers in mouse embryonic versus injury-activated epicardial cells differ quite significantly.[26] Given the essential roles of the epicardium during both development and regeneration, surprisingly little is known about the upstream transcriptional regulation driving epicardial gene expression programs during either process. Efficient and precise gene expression is controlled by TFs, which bind to specific DNA sequences within promoters and distal *cis*-regulatory elements. Enhancers, short regions of open chromatin, make up the most abundant subset of non-promoter *cis*-regulatory elements.[27] The regulatory activity of genomic regions is dependent on how closely they are structurally associated with

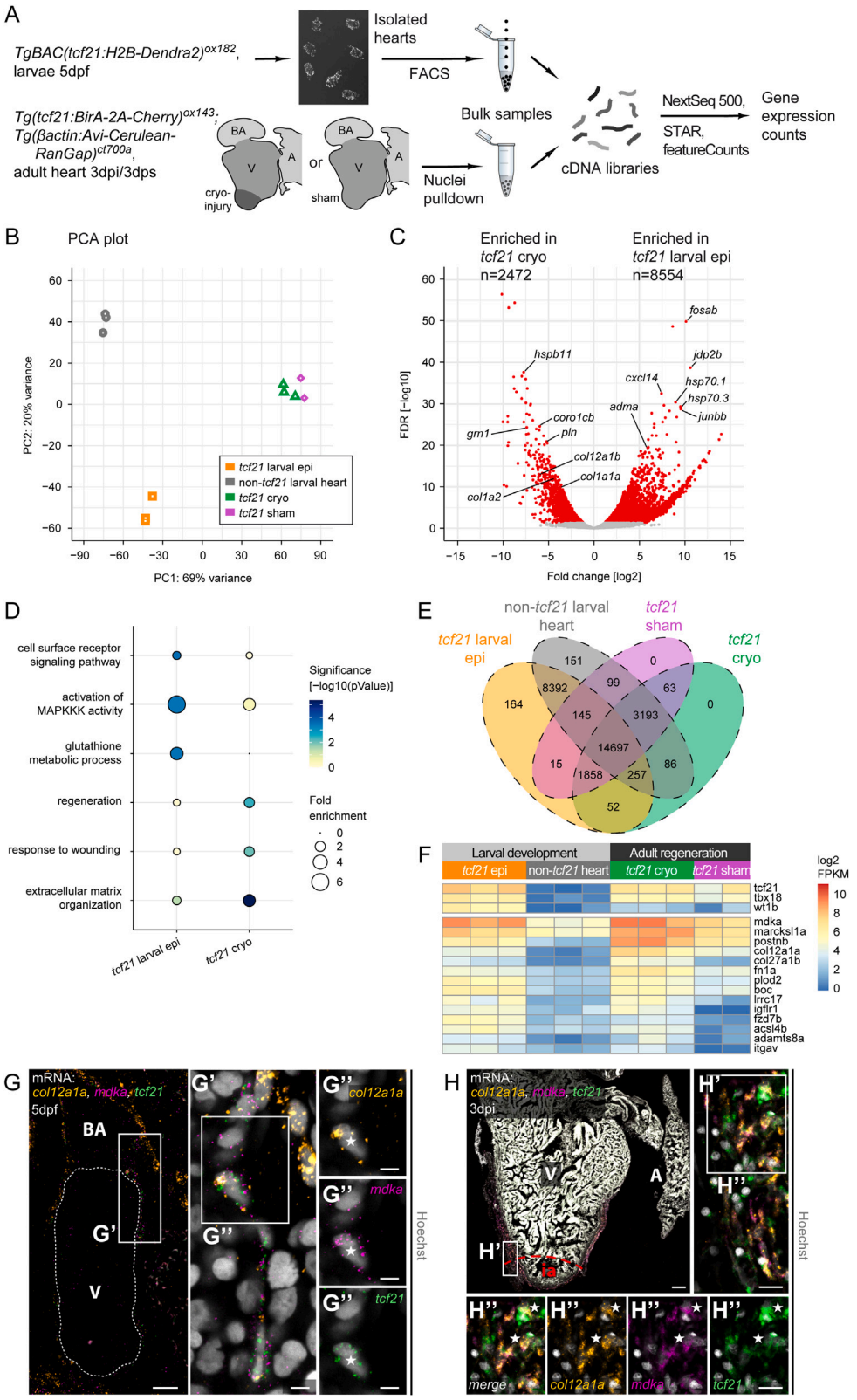

Figure 1. Gene expression programs in the developing and regenerating zebrafish epicardia are distinct

(A) Overview of the RNA sequencing workflow.

(B) Principal-component clustering of transcriptome samples.

(legend continued on next page)

neighboring nucleosomes because this affects the capacity of TFs to bind.[28] By mapping open chromatin regions across the genome, for example, via assay for transposase-accessible chromatin (ATAC)-sequencing,[29] it is possible to identify potential active regulatory elements. Recently, regions in the zebrafish genome have been identified as tissue regeneration enhancer elements (TREEs), becoming activated upon cardiac injury.[30–34] Epicardial TREEs have been identified in the mouse[35,36] and recently in the adult zebrafish heart following resection of the ventricle.[37] However, gene regulation in the adult zebrafish epicardium following cardiac injury has not been systematically compared with that in the developing epicardium.

Here, we compared the transcriptome and epigenome of developing and regenerating zebrafish epicardia. We found that the epicardial transcriptomic programs deployed during development and regeneration are distinct and that regeneration only partially recapitulates development. Intriguingly, even the underlying genetic programs driving the expression of a small cohort of shared transcripts in the developing and post-injury epicardium showed recognizable differences.

By integrating transcriptional and epigenomics datasets, we built gene regulatory networks and inferred Wt1a, Wt1b, and the activator protein-1 (AP-1) subunits Junbb, Fosab, and Fosb as central regulators of the developing epicardial network, while TFs such as Hif1ab, Nrf1, Tbx2b, and Zbtb7a featured as putative central regulators of the regenerating epicardial network. We used an electroporation-based approach to deliver CRISPR-Cas9 components into the epicardium of the injured heart to induce loss of function specifically during heart regeneration. Targeting *hif1ab*, *nrf1*, *tbx2b*, and *zbtb7a* via this approach led to significantly increased numbers of *tcf21*$^{+}$ cells in both the wound and distal ventricle, accompanied by an excess in fibrosis at a later stage after injury. These results demonstrate the functional importance of the epicardial regulatory core that comprises Hif1ab, Nrf1, Tbx2b, and Zbtb7a during zebrafish heart regeneration.

RESULTS

Gene expression profiles of the developing and regenerating zebrafish epicardia are largely distinct

To compare the epicardial gene expression profiles during zebrafish development and following adult heart injury, we analyzed transcriptional profiles of epicardial cells derived from *TgBAC(tcf21:H2B-Dendra2)*^{ox182} and *TgBAC(tcf21:BirA-2a-mCherry)*^{ox143}; *Tg(βactin:Avi-Cerulean-RanGap)*^{ct700a} transgenic lines. We obtained bulk RNA sequencing data at 5 days post fertilization (dpf), a time point when the epicardium is fully formed, from cardiac *tcf21*:H2B-Dendra2-positive cells (*tcf21* larval epi) and *tcf21*:H2B-Dendra2-negative heart cells (non-*tcf21* larval heart) (Figures 1A and S1A). For adult samples, we profiled cardiac *tcf21*:BirA-2a-mCherry; *βactin*:Avi-Cerulean-RanGap^{+} nuclei at 3 days post cryoinjury (dpi) (*tcf21* cryo), a time point when the activation of the injured epicardium is organ wide,[3] using the biotagging approach to isolate specific nuclei.[38,39] The developing epicardium at 5 dpf resembles the regenerating epicardium at 3 dpi in terms of expressing factors such as *tbx18* and *wt1b*, which are not expressed in the adult uninjured epicardium. We further processed corresponding sham-control samples at 3 days post sham injury (dps) (*tcf21* sham). Principal-component analysis (PCA) showed that the variability of gene expression between replicates of each condition was low (Figure 1B). The majority of variability was due to differences between larval and adult samples (PC1, 69%). Directly comparing *tcf21* larval epi and *tcf21* cryo, we found that 8,554 genes were significantly enriched in the larval epicardium, while 2,472 genes were enriched in the adult cryoinjured epicardium (Figure 1C). Among the genes enriched in the larval epicardium were the chemokine ligand *cxcl14* and the AP-1 TF subunits *fosab*, *junbb*, and *jdp2b*. The adult cryoinjured epicardium featured several enriched collagens, such as *col1a1a*, *col1a2*, and *col12a1b*.

Genes enriched in *tcf21* larval epi were associated with multiple Gene Ontology (GO) terms related to cellular signaling, such as "cell-surface receptor signaling pathway" ($p = 0.00029$) and "activation of MAPKKK activity" ($p = 0.00037$) (Figure 1D). Genes enriched in *tcf21* cryo were associated with injury-related processes such as "regeneration" ($p = 0.00384$), "response to wounding" ($p = 0.00972$), and "ECM organization" ($p = 4.2 \times 10-6$).

After assessing the transcriptomic differences between developing and regenerating epicardia, we next asked whether there was a common transcriptomic program. We compared gene expression in *tcf21* larval epi with that in the non-*tcf21* larval heart and intersected this comparison with that of *tcf21* cryo versus *tcf21* sham (Figure 1E). A cohort of 52 genes enriched in adult cryoinjured versus sham-control epicardium was also enriched in larval epicardium versus larval control (Figure 1E; Table S1). Many of these genes were components of the ECM or signaling factors (Figure 1F), and several have been implicated in heart regeneration previously, such as *fn1a*.[17] The cytokine midkine *a* (*mdka*) was shown to be expressed in the zebrafish epicardium following injury, acting as a regulator of fibrosis.[40]

(C) Differential gene expression analysis of *tcf21* larval epi versus *tcf21* cryo. Shown are $\log_2$-transformed expression fold changes and Benjamini-Hochberg-adjusted Wald test p values. Significantly enriched genes (adjusted p value < 0.05) are colored in red.
(D) GO term over-representation of genes enriched in *tcf21* larval epi (versus *tcf21* cryo, left column) and genes enriched in *tcf21* cryo (right column). Bubble size depicts the magnitude of statistical enrichment, color significance.
(E) Venn diagram depicting the overlap of gene expression enrichment across conditions. Indicated are the numbers of genes contained in each intersection.
(F) Expression of genes enriched in *tcf21* larval epi versus non-*tcf21* larval heart and enriched in *tcf21* cryo versus *tcf21* sham.
(G) mRNA staining of *col12a1a* (orange), *mdka* (magenta), and *tcf21* (green) in a 5 dpf heart. (G′ and G′′) A nucleus (asterisk) in the epicardial region surrounded by *col12a1a*, *mdka*, and *tcf21* transcripts.
(H) mRNA staining of *col12a1a* (orange), *mdka* (magenta), and *tcf21* (green) in a 3-dpi heart. Ia, injury area. (H′ and H′′) Single nuclei (asterisks) in the epicardial region surrounded by *col12a1a*, *mdka*, and *tcf21* transcripts.
Scale bars: 100 μm in (H); 20 μm in (G), (H′), and (H′′); and 5 μm in (G′) and (G′′). Color channels adjusted separately for brightness/contrast. (G) and (H) are single optical sections. dpf, days post fertilization; dpi, days post-injury; V, ventricle; A, atrium; BA, bulbus arteriosus. Number of biological replicates analyzed: *tcf21* larval epi, n = 3; non-*tcf21* larval heart, n = 3; *tcf21* cryo, n = 3; *tcf21* sham n = 2. See also Figure S1.

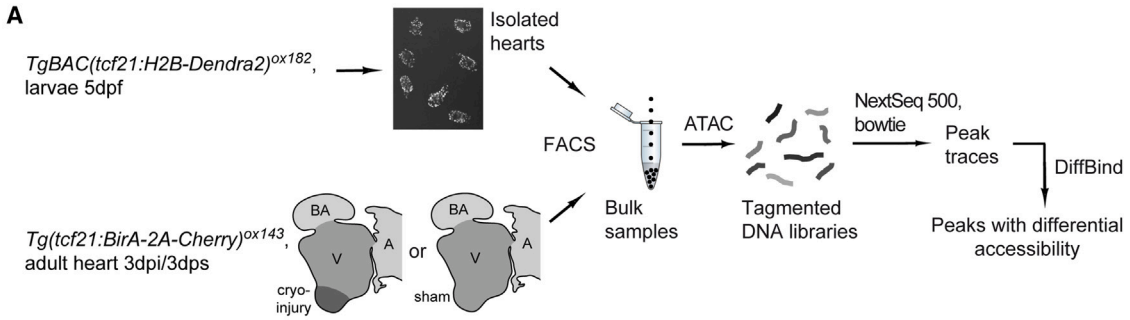

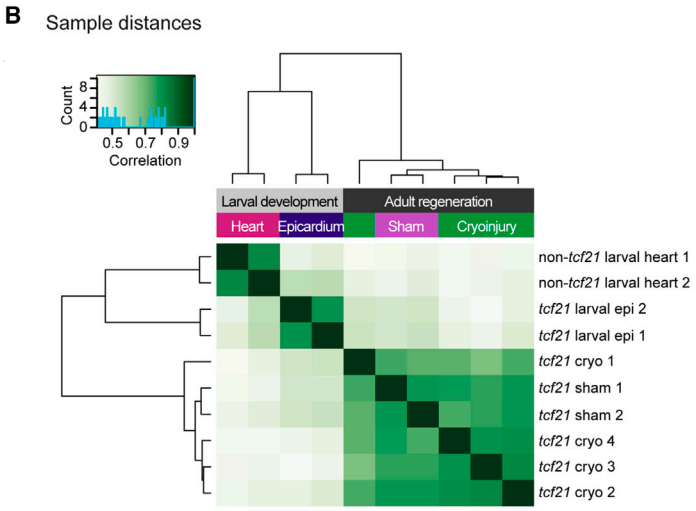

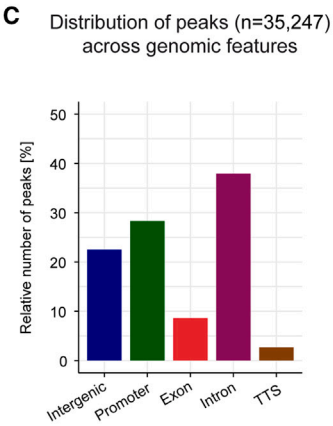

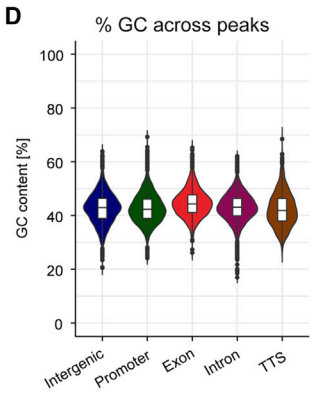

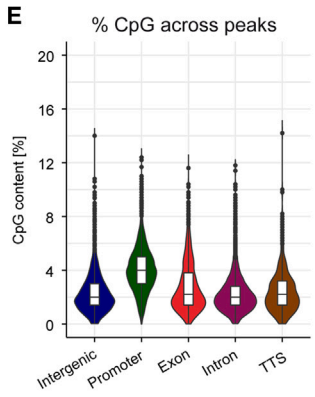

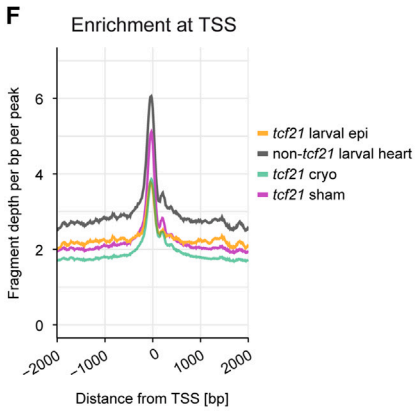

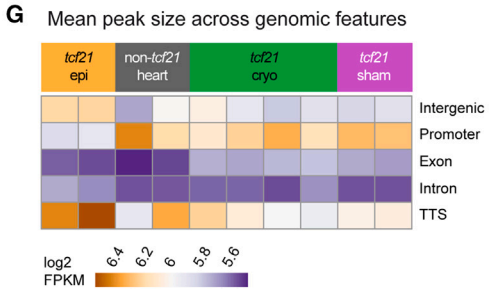

(legend on next page)

Collagen 12a1a (*col12a1a*) and *periostin b* (*postnb*) were also elevated in expression following zebrafish heart injury.[15,41] However, other members of the 52 genes have not been described in a cardiac injury context before, for example, the actin bundling protein *myristoylated alanine-rich c-kinase substrate like 1a* (*marcksl1a*)[42] and the collagen processing enzyme *procollagen-lysine, 2-oxoglutarate 5-dioxygenase 2* (*plod2*).[43]

Using multiplexed hybridization chain reaction (HCR) *in situ* staining,[44] we validated the expression of some of the shared transcripts in developing (Figures 1G and S1B) and cryoinjured epicardium (Figures 1H and S1C). We found *mdka* and *col12a1a* (Figures 1G and 1H), as well as *postnb* (Figures S1B and S1C), expressed within developing and regenerating epicardial cell layer, co-localizing with *tcf21* transcripts. HCR also identified the expression of *mdka* and *col12a1a* in sham-treated adult epicardium (Figure S1D), in line with the transcriptomic data.

In summary, our data suggest that the epicardial transcriptomic response deployed upon adult heart cryoinjury at 3 dpi is not a mere recapitulation of the developmental epicardial gene program (see Figure S1E for top genes enriched in either larval or cryoinjured epicardium). However, we also identified several transcripts shared by developing and regenerating epicardia, suggesting that these genes might represent essential regulators of epicardial function.

Chromatin accessibility profiles of the developing and regenerating epicardia

Next, we sought to gain insight into the genomic regulation that underlies epicardial gene expression.We performed ATAC-seq on fluorescence-activated cell (FAC)-sorted 5-dpf *tcf21*$^{+}$ epicardial cells (isolated from *TgBAC(tcf21:H2B-Dendra2)*^{ox182}), corresponding *tcf21*$^{-}$ non-epicardial heart cells; adult 3-dpi *tcf21*$^{+-}$ epicardial cells (isolated from *TgBAC(tcf21:BirA-2a-mCherry)*^{ox143}); and *tcf21*$^{+}$ cells from corresponding sham-control samples (isolated from *TgBAC(tcf21:BirA-2a-mCherry)*^{ox143}) (Figure 2A).

Following identification of accessible chromatin regions (peaks) across the genome,[45] we clustered all samples according to the similarity of their peak positions[46] (Figure 2B). The biological replicates of each condition clustered closely together. However, *tcf21* cryo peak profiles did not correlate well with those of *tcf21*:H2B-Dendra2^{+} larval epicardial samples (*tcf21* larval epi) or with those of *tcf21*:H2B-Dendra2^{-} larval heart cells (non-*tcf21* larval heart).

We next constructed a consensus peak set of 35,247 accessible regions across all conditions[46] and analyzed peak genomic features using Homer[47]; 74.8% of the peaks resided in promoters or gene coding regions (Figure 2C), suggesting that they might be involved in the proximal regulation of transcriptional activity, whereas 22.5% resided in intergenic regions. The median GC content varied between 42% and 45% across peaks (Figure 2D), which is in the range of previously reported values for the zebrafish genome.[48] The median peak sequence proportion occupied by elongated GC-rich regions (CpG islands) ranged from 3% to 5%, with peaks in promoters displaying the highest median CpG content (Figure 2E), in line with the well-established connection between CpG islands and transcriptional start sites (TSSs).[49] Furthermore, the average read coverage per condition in regions surrounding TSS was elevated, as expected (Figure 2F). We computed average peak sizes and found that promoter peaks were larger than other peaks in all conditions except the larval epicardium (t test, promoter versus non-promoter peaks: *tcf21* larval epi, $p = 0.75$; non-*tcf21* larval heart, $p = 5.8 \times 10^{-102}$; *tcf21* cryo, $p = 5.3 \times 10^{-105}$; *tcf21* sham, $p = 2.4 \times 10^{-167}$) (Figure 2G). The fact that promoter peaks were smaller in *tcf21* larval heart than in *tcf21* cryo might indicate that epicardial gene regulation is less dependent on promoters during development. Conversely, peaks located in the proximity of the transcriptional termination site (TTS) and intergenic peaks were larger in *tcf21* larval epi than in *tcf21* cryo. These observations suggest that the regulation of gene expression in the developing epicardium differs extensively from that in the injured adult epicardium.

Epicardial gene expression during development and regeneration depends on distinct regulatory programs

Given that our data implicate distinct epicardial transcriptomic programs during development and regeneration, we next investigated the regulatory programs underlying such differences. By directly comparing *tcf21* larval epi and *tcf21* cryo, we identified 3,211 peaks (10%) with enriched accessibility in *tcf21* larval epi and 554 peaks (2%) with enriched accessibility in *tcf21* cryo (Figure 3A); 4 out of 8 peaks located in the *tcf21* locus were among those significantly enriched in *tcf21* cryo, with 3 out of 4 peaks located less than 10 kb from the *tcf21* TSS (Figure 3B). Furthermore, when averaged across replicates, 7 out of the 8 peaks annotated to *tcf21* showed higher accessibility in the regenerating epicardium. This suggests that the regulation of *tcf21* expression in the regenerating epicardium might utilize a more complex web of different regulatory elements, allowing for a more rapid response to injury than the transcriptional regulation deployed during development.

We found that *tcf21* larval epi enriched peaks featured a lower proportion of promoter peaks than *tcf21* cryo enriched peaks (Figure 3C, *tcf21* larval epi: 10%, *tcf21* cryo: 26%). In contrast, intergenic peaks showed the opposite trend (intergenic, *tcf21* larval epi: 33%, *tcf21* cryo: 23%), suggesting a shift from a distal regulation in the developing epicardium toward a more promoter-based regulation in the regenerating epicardium. While developmental GO terms such as "embryonic morphogenesis"

Figure 2. Chromatin accessibility in the developing and regenerating zebrafish epicardia

(A) Overview of the ATAC sequencing workflow.

(B) Distance-based clustering of the Pearson correlations of larval and adult accessible chromatin profiles, as indicated by the dendrogram. Correlation values are indicated by color.

(C–E) Relative quantification of peak distribution across genomic features (C), peak GC content (D), and peak CpG content (E).

(F) Average relative sequencing read densities at TSSs.

(G) Average peak size across genomic features.

dpf, days post fertilization; dpi, days post-injury; V, ventricle; A, atrium; BA, bulbus arteriosus; bp, base pairs. Number of biological replicates analyzed: *tcf21* larval epi, n = 2; non-*tcf21* larval heart, n = 2; *tcf21* cryo, n = 4; *tcf21* sham, n = 2. In D,E, box and whiskers plots (in the style of Tukey) indicate median and first/third quartiles.

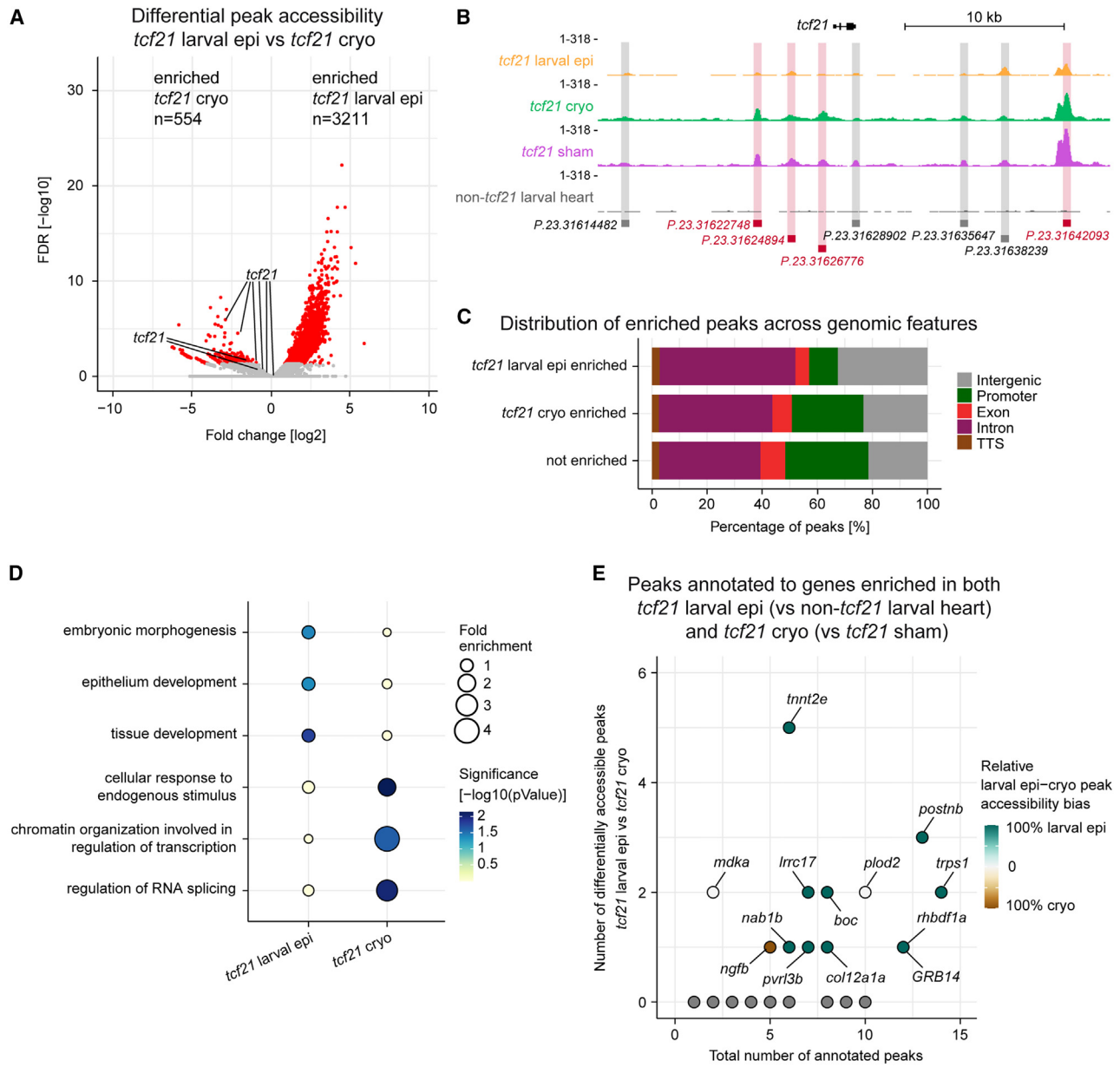

Figure 3. Distinct chromatin accessibility profiles in the developing and regenerating epicardia

(A) Differential peak accessibility analysis, comparing *tcf21* larval epi with *tcf21* cryo. Shown are $\log_2$-transformed accessibility fold changes and Benjamini-Hochberg-adjusted Wald test p values. Significantly enriched peaks (adjusted p value < 0.05) are colored in red. Highlighted are peaks located in the *tcf21* locus.

(B) Chromatin accessibility in the *tcf21* locus. Peaks significantly enriched in cryoinjured versus larval epicardium are highlighted in red.

(C) Relative quantification of differentially accessible peak distribution across genomic features.

(D) GO term over-representation of genes located close to peaks enriched in *tcf21* larval epi (left column) or *tcf21* cryo (right column). Bubble size depicts the magnitude of statistical enrichment, color significance.

(E) Differential accessibility of peaks located in the vicinity of marker genes of larval and adult cryoinjured epicardium (n = 52), quantified on gene level. Bubble color indicates the ratio of the number of differentially accessible peaks enriched in *tcf21* larval epi versus the number of peaks enriched in *tcf21* cryo (green = all *tcf21* larval epi, brown = all *tcf21* cryo, white = equal ratio).

(p = 0.04) and "tissue development" (p = 0.016) were over-represented for the *tcf21* larval epi condition (Figure 3D), the top over-represented terms for the *tcf21* cryo elements were associated with cellular responses, such as "cellular response to endogenous stimulus" (p = 0.007), and gene regulation, such as "chromatin organization involved in regulation of transcription" (p = 0.024), potentially reflecting the response to injury.

Next, we investigated to what extent chromatin accessibility in the vicinity of the 52 genes expressed in developing and regenerating epicardia (Table S1) varied between these conditions. 13 of these genes featured differentially accessible peaks with a

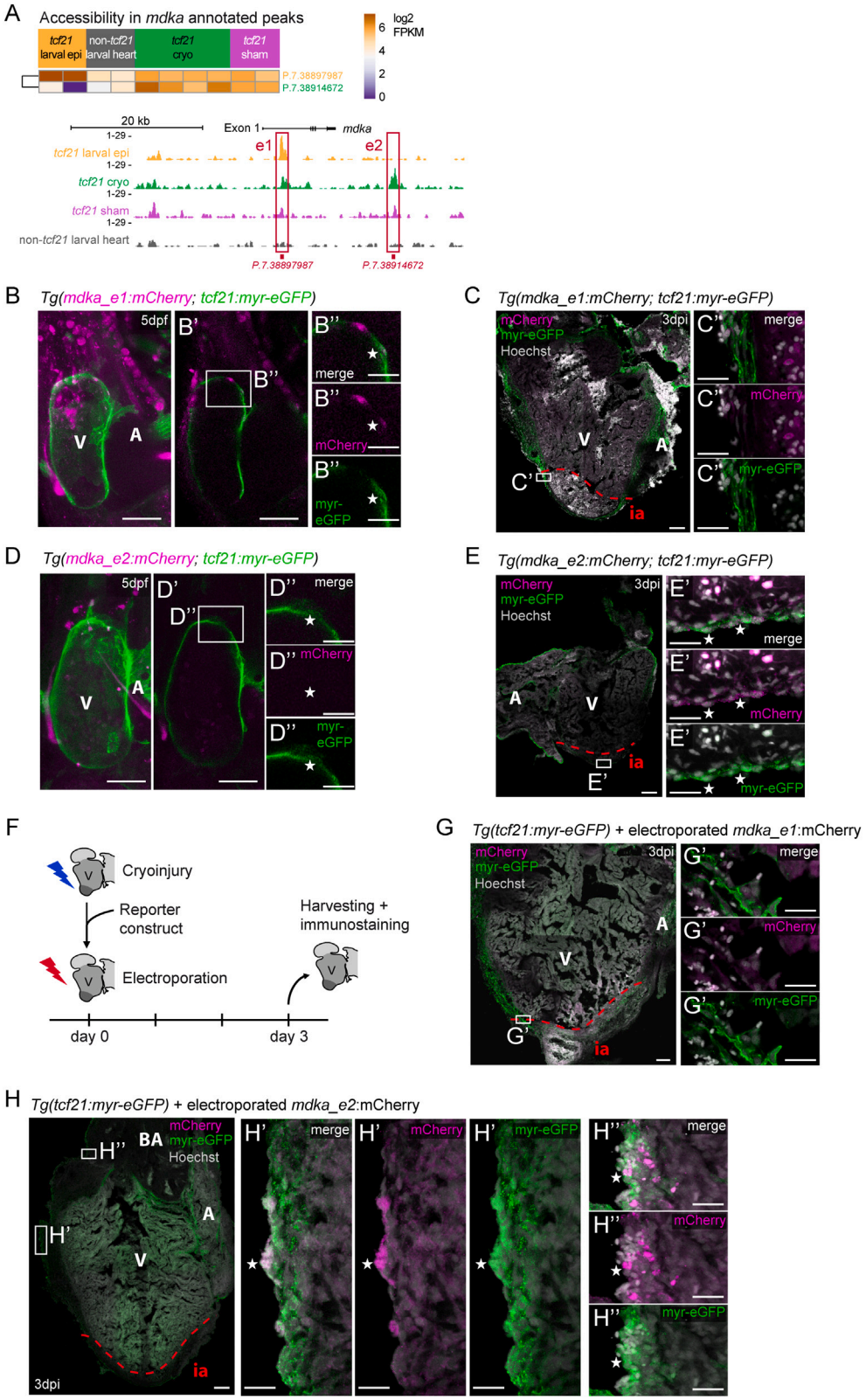

(legend on next page)

strong bias toward enrichment in the developing epicardium (Figure 3E), indicating differences in the regulation of gene expression even for genes that label both developing and regenerating epicardia.

Finally, we tested the *in vivo* activity of differentially accessible elements located close to *mdka* and *col12a1a*, two of the genes expressed in both developing and regenerating epicardia. Establishing stable Ac/Ds fluorescent reporter lines,[50] we found that *mdka_e1*, a peak enriched in *tcf21* larval epi and located within the first intron of *mdka* (Figure 4A), was active in the developing epicardium (Figure 4B) but inactive in the adult epicardium after cryoinjury (Figure 4C). In contrast, *mdka_e2*, a peak enriched in *tcf21* cryo and located 10 kb downstream of *mdka* (Figure 4A), showed no activity in the developing epicardium (Figure 4D) but was active in a subset of adult epicardial cells following heart injury (Figure 4E).

We also validated the enhancer activity of *mdka_e1* and *mdka_e2* using a transient approach, adapting an *in vivo* DNA electroporation protocol previously used in zebrafish.[51] We initially electroporated a DNA construct encoding ubiquitously expressed Citrine into an uninjured heart and observed widespread fluorescence in the epicardial region (Figure S2A). We next performed cryoinjury on *Tg(tcf21:myr-eGFP)*^{ox183} fish and subsequently electroporated the *mdka* enhancer reporter vectors used to create stable expression lines (Figure 4F). While we did not detect fluorescence in the adult epicardium after cryoinjury when electroporating the *mdka_e1* reporter construct (Figure 4G), we found clear epicardial *mdka_e2* enhancer activity (Figure 4H), matching the results obtained using the stable reporter lines. Thus, the electroporation approach enables enhancer activity in the regenerating adult zebrafish heart to be tested in transient.

In addition, we analyzed a peak enriched in *tcf21* larval epi and located 30 kb downstream of *col12a1a* (*col12a1a_e1*, Figure S2B). A stable *col12a1a_e1* reporter line indicated enhancer activity in both the developing and the regenerating epicardium (Figures S2C and S2D).

Together, our data show that gene expression changes observed in the developing and regenerating epicardia are likely to be attributable to differences in open chromatin dynamics.

Development-specific and regeneration-specific epicardial gene regulatory networks identify central regulators of epicardial gene expression

We next sought to understand which TF might regulate epicardial gene expression during heart development and regeneration. For this, we queried our ATAC-seq peak set for the presence of 746 vertebrate TF binding motifs obtained from the JASPAR 2020 database.[52] We jointly analyzed chromatin accessibility and motif occurrence using chromVAR[53] and clustered our ATAC-seq samples according to the accessibility deviations of all motifs (Figure S3A). Similar to the peak accessibility-based clustering (Figure 2B), *tcf21* larval epi samples clustered away from adult *tcf21* cryo and sham samples (Figure S3A).

We next queried TF motif presence in peaks differentially accessible in developing versus regenerating epicardia. We found the increased presence of FOS and JUN binding motifs, subunits of the AP-1 complex, in peaks enriched in *tcf21* cryo (Figure 5A). The AP-1 complex is required for zebrafish heart regeneration and controls chromatin accessibility in cardiomyocytes.[54] In contrast, WT1 and KLF2 motifs were more frequent in peaks enriched in *tcf21* larval epi. These results are consistent with the recent finding that accessibility of AP-1 binding sites in the adult zebrafish epicardium increases following injury, whereas accessibility of WT1 binding sites decreases.[37] TCF21 and TBX18 motifs were present at equal frequencies in both conditions. Thus, distinct TFs might regulate the larval and the injured adult epicardia. Therefore, we analyzed TF expression (Figure 5B), including a recently published expression data from *tcf21*$^{+}$ cells in the adult uninjured heart.[55] We found that *wt1a* and *wt1b* expression was enriched in larval versus regenerating epicardia (false discovery rate [FDR](*wt1a*) = 0.0016, FDR(wt*1b*) = 2×10^{-8}), matching the increased WT1 motif accessibility. However, we found that AP-1 complex components were also enriched in the developing epicardium (FDR(*jun*) = 9×10^{-12}, FDR(junba) = 5×10^{-19}, FDR(junbb) = 2×10^{-29}, FDR(*fosl1a*) = 3×10^{-5}, FDR(fosab) = 1×10^{-50}, FDR(fosb) = 3×10^{-12}). These findings contrast with the lower accessibility of AP-1 binding sites in larval-enriched peaks. Genes enriched in the regenerating epicardium included *hypoxia-inducible factor 1ab* (*hif1ab*) (FDR = 0.0052), shown to be required for zebrafish heart regeneration;[56] the zinc-finger and BTB domain-containing factor *zbtb7a* (FDR = 3×10^{-9}), a regulator of genes associated with heart failure following myocardial infarction[57]; and *tbx2b* (FDR = 1×10^{-6}), a known regulator of atrioventricular canal formation.[58] Generally, these genes were lowly expressed in the adult uninjured epicardium, indicating that they are not involved in maintaining the intact epicardium.

We next constructed epicardial gene regulatory networks, combining chromatin accessibility and gene expression data

Figure 4. *In vivo* enhancer activity of differentially accessible chromatin regions in the *mdka* locus

(A) Accessibility of peaks close to *mdka*. Red frames indicate peaks analyzed further in (B), (C), and (G) (e1) and (D), (E), and (H) (e2).

(B) Stable *mdka_e1*-driven mCherry expression (magenta) at 5 dpf. Expression of *tcf21* is indicated by myr-eGFP fluorescence (green membranes). (B′) Single optical section from (B). (B″) mCherry fluorescence in the epicardium (asterisk).

(C) Stable *mdka_e1*-driven mCherry expression in the adult cryoinjured heart at 3 dpi. (C′) High magnification image of a part of the injury area (ia) in (C).

(D) Stable *mdka_e2*-driven mCherry expression (magenta) at 5 dpf. (D′) Single optical section from (D). (D″) mCherry fluorescence in the epicardium (asterisk) is absent.

(E) Stable *mdka_e2*-driven mCherry expression in the adult cryoinjured heart at 3 dpi. (E′) High magnification image of a part of the injury area in (E). An epicardial cell showing *mdka_e2* activity is denoted by an asterisk.

(F) Workflow of adult zebrafish heart injury followed by electroporation of enhancer activity reporter constructs.

(G and H) Transient mCherry expression driven by *mdka_e1* (G) or *mdka_e2* (H) following electroporation into the cryoinjured adult heart. (G′, H′, and H″) High magnification images of (G) and (H). In (H′) and (H″), epicardial cells showing *mdka_e2* activity are denoted by asterisks.

Scale bars: 100 μm in (C), (E), (G), and (H); 50 μm in (B), (B′), (D), and (D′); and 20 μm in (B″), (C′), (D″), (E′), (G′), (H′), and (H″). In (A), yellow: enrichment *tcf21* larval epi, green: enrichment *tcf21* cryo. (B) and (D) show endogenous fluorescence, (C), (E), (G), and (H) show immunefluorescence. V, ventricle; A, atrium; BA, bulbus arteriosus. See also Figure S2.

CellPress
OPEN ACCESS

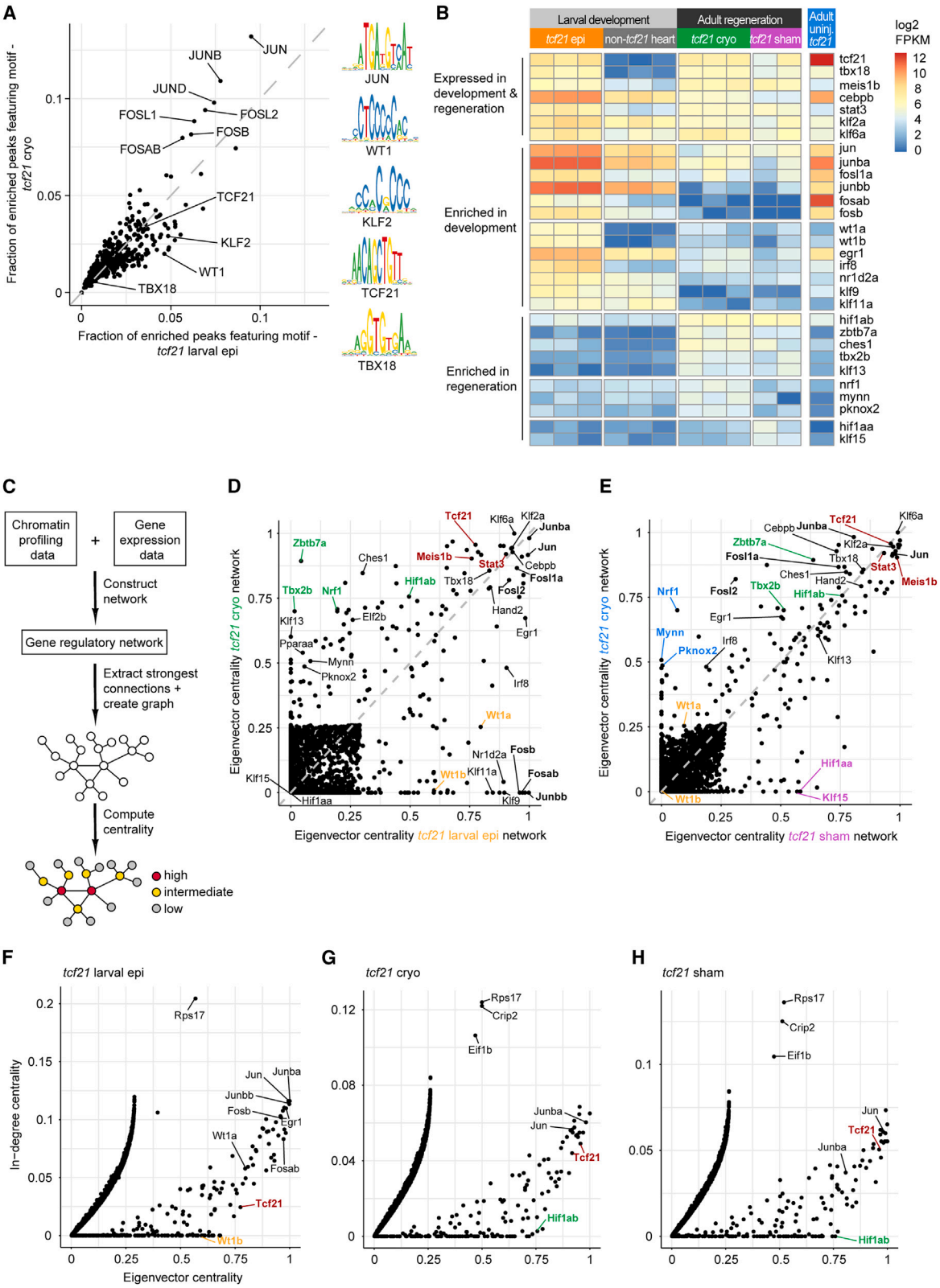

Figure 5. Gene regulatory networks identify central transcriptional regulators in the developing and regenerating zebrafish epicardia

(A) Quantification of TF motif presence in differentially accessible peaks in *tcf21* larval epi versus *tcf21* cryo. Selected motif logos are shown on the right.

(B) Expression of TFs in larval, adult cryoinjured, and sham-treated epicardia.

(legend continued on next page)

using a recently developed computational framework[59] (Figure 5C). We subset networks to the strongest 1% of connections, yielding sub-networks of approximately 100,000 connections (Figure S3B). All sub-networks featured 200–250 TFs (n [larval epicardium] = 230, n[cryoinjured epicardium] = 216, n [sham-treated epicardium] = 214) and a higher number of target genes (n[larval epicardium] = 1,798, n[cryoinjured epicardium] = 2,445, n[sham-treated epicardium] = 2,422) (Figure S3C). To predict the connectivity within the network and thereby the regulatory importance of TFs, we computed the eigenvector centrality of each factor.[60] Tcf21, Stat3, and Meis1b, as well as Jun, Junba, Fosl1a, and Fosl2, possessed high centrality values in larval and cryoinjured epicardial networks, indicating that they might regulate epicardial transcription in both contexts (Figure 5D). In contrast, TFs such as W1a and Wt1b were much more central in the developing epicardial network than in the regenerating network, while TFs including Hif1ab, Zbtb7a, Tbx2b, and Nrf1 showed the opposite trend. To further identify TFs that might play a regulatory role specifically during heart regeneration, we compared centrality between cryoinjured and sham-treated epicardial networks (Figure 5E). Nrf1, Mynn, and Pknox2 featured high centrality specifically in the cryoinjured epicardial network, while Klf15, Hif1aa, and others showed higher centrality in the sham network. We then asked whether TFs with high network centrality were also positioned at the top of the regulatory TF hierarchy. To this end, we compared eigenvector centrality to in-degree centrality (IDC, a measure of the number of incoming network connections).[60] Wt1b (IDC = 0), but not Jun (IDC = 0.116) and Fosab (IDC = 0.083), were among the TFs predicted to reside at the top of the regulatory hierarchy in the larval epicardium (Figure 5F). In contrast, Hif1ab was predicted to reside at the top of the hierarchies in the adult epicardial conditions (IDC[cryoinjured] = 0.003, IDC[sham-treated] = 0) (Figures 5G and 5H). Interestingly, *tcf21* was predicted to receive a lower amount of regulatory input in the larval epicardium than in the adult activated epicardium (IDC[larval] = 0.024, IDC[cryoinjured] = 0.049, and IDC[sham-treated] = 0.051), suggesting Tcf21 might play a more downstream role during heart regeneration.

In summary, our gene regulatory network analysis predicts specific TFs that play a central role in regulating epicardial gene expression (see Figure S4A for a complete overview).

Specific sets of epicardial upstream regulators drive post-injury transcriptional reactivation of developmental genes

After defining TFs that are epicardial regulators during development and regeneration, we asked whether the small set of developmental genes re-activated upon injury is differentially regulated (as suggested in Figure 3E). To this end, we compared the scaled strength of network connections between these genes (Table S1) and Tcf21, Meis1b, Stat3 (predicted to be central in the epicardium during heart development and regeneration), Wt1a, and W1b (more central in the developing epicardium), as well as Tbx2b and Nrf1 (more central in the regenerating epicardium) (Figures 6A and 6B). We found that Tcf21, Meis1b, and Stat3 had high connection scores in both larval and cryoinjured epicardial networks. However, Wt1a and Wt1b mainly exhibited stronger connections in the larval epicardial network, while Tbx2b and Nrf1 generally featured stronger connections in the cryoinjured epicardial network. This analysis suggests that even for transcripts present during both development and regeneration, divergent sets of upstream TFs regulate their expression.

We next assessed which TFs might drive *in vivo* larval cardiac activities of *mdka_e1* and *col12a1a_e1*. In both enhancer sequences, we identified a WT1 binding motif (*mdka_e1*: CTCCTCCCCCATGC, forward strand, motif score = 10.8, *col12a1a_e1*: ATGTGTGGGAGGAA, reverse strand, motif score = 11.1) (Figures 6C and S5A). In addition, the *mdka_e1* sequence featured a KLF9 motif (TGTGTGTGTGTGTCTC, reverse strand, motif score = 10.3) and a MEIS1 motif (AGTGATTTATGAC, reverse strand, motif score = 10.9). The *mdka_e2* sequence, accessible mostly in the cryoinjured epicardium, featured many binding sites of TFs with high centrality in the *tcf21* cryo subnetwork, including a TBX2 motif (TTTGACACCCT, reverse strand, motif score = 8.9) (Figure 6D). We found the DNA binding domains of human TBX2 and zebrafish Tbx2b possess a 96% amino acid sequence similarity (Figure S5B), suggesting that Tbx2b may bind to the TBX2 binding motif. Multiplexed *in situ* staining validated the expression of *klf9* in the developing epicardium (Figure 6E), with sparse expression in the injury area following cryoinjury (Figure S5C). Expression of *tbx2b* was prominent in the cryoinjured adult heart, co-localizing with *tcf21* transcripts in the injury area (Figure 6F), whereas the expression of *tbx2b* in the larval heart seemed mostly confined to the atrium (Figure S5D). We detected the expression of *meis1b* in both the larval and the adult injured hearts, co-localizing with *tcf21* transcripts, as well as *sox4a* transcripts (Figures S5E and S5F). Finally, we found that *zbtb7a* and *nrf1* were sparsely expressed within the larval epicardium, with more prominent expression in the adult injury area close to *tcf21* (Figures S5G and S5H). In line with our results, a recent publication found ZBTB7A motif accessibility increased in zebrafish epicardial cells upon cardiac injury.[37]

Taken together, our analysis identified TFs that might drive differential regulation of genes commonly expressed in developing and regenerating zebrafish epicardia.

To focus on epicardial upstream regulation, we visualized the strongest connections between Tcf21, Meis1b, Stat3, Wt1a, Wt1b, Hif1ab, and Nrf1 in both networks (Figures 6G and 6H) and found striking differences. While Wt1b was positioned at the top of the regulatory hierarchy in the larval epicardial condition, it was absent from the cryoinjured epicardial condition. In

(C) Workflow to construct gene regulatory networks and to identify central regulators.
(D and E) Eigenvector centrality in *tcf21* larval epi and *tcf21* cryo networks (D) and in *tcf21* sham and *tcf21* cryo networks (E). TFs with enriched centrality in cryoinjured epicardium are shown in blue, TFs with enriched centrality in sham-treated epicardium in purple.
(F–H) In-degree centrality versus eigenvector centrality in *tcf21* larval epi (F), *tcf21* cryo (G), and *tcf21* sham (H) sub-networks.
In (D–H), selected regulators of both larval and adult epicardium are shown in red, regulators of larval epicardium in yellow, regulators of adult epicardium in green. In (D) and (E), AP-1 components are labeled in bold letters. Epi, epicardium. See also Figures S3 and S4.

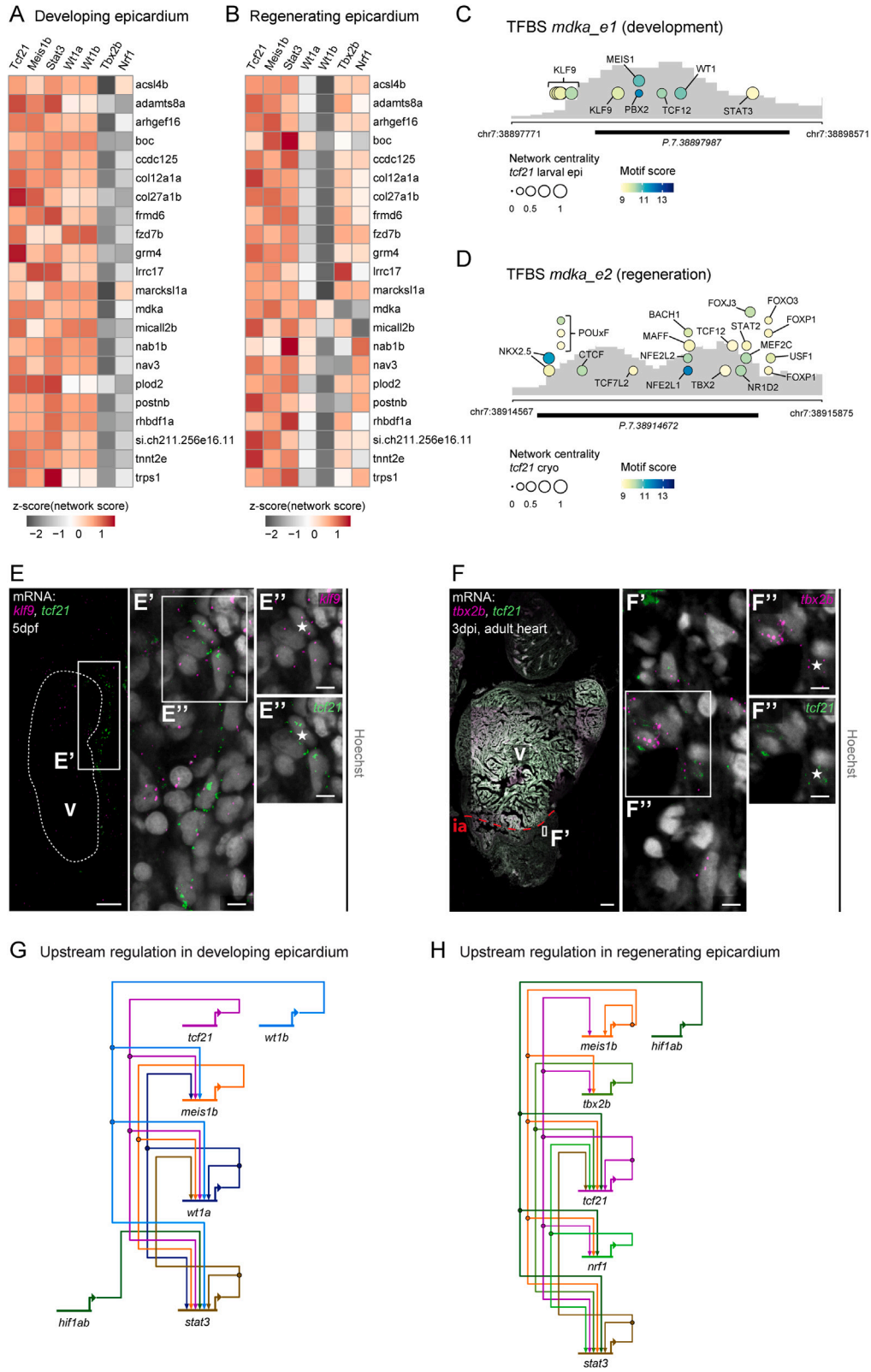

Figure 6. Differential transcriptomic regulation of genes expressed in both developing and regenerating zebrafish epicardia

(A and B) Network connection scores within the network representing the developing epicardium (A) and that representing the regenerating epicardium (B) between selected TFs and genes expressed in both conditions.

(legend continued on next page)

contrast, Hif1ab only played a marginal role in larval epicardial regulation but was well connected in epicardial regulation upon injury. Hif1ab, for example, connected to Nrf1, another regulator exclusively featuring in the upstream regulation during regeneration. Matching the low IDC in the larval epicardial network (Figure 5F), Tcf21 resided at the top of the TF hierarchy regulating the developing epicardium. However, in the regulatory network of the cryoinjured epicardium, Tcf21 received regulatory input from multiple sources, including itself. This might reflect a need to rapidly upregulate *tcf21* expression following injury, contrasting with a more steady-state expression in the developing epicardium. Thus, the predicted upstream transcriptional regulation in the developing epicardium differed markedly from that in the regenerating epicardium.

Loss of function of core regulators of the adult regenerating epicardium affects zebrafish heart regeneration

We went on to ask whether the core transcriptional regulators in the adult regenerating epicardium identified *in silico* indeed play a functional role during zebrafish heart regeneration. To this end, we induced Cas9-mediated gene editing via electroporation at the time of cryoinjury. Co-electroporating a plasmid driving Cas9 expression and a sgRNA targeting *eGFP* (Figure S6A) substantially disrupted epicardial fluorescence in *TgBAC(tcf21:myr-eGFP)*^{ox183} hearts (Figures S6B and S6C), indicating efficient gene editing in the epicardium.

We then targeted the genes encoding four TFs with high centrality in the *tcf21* cryo network (Figure 5D): *hif1ab*, *nrf1*, *tbx2b*, and *zbtb7a*. Simultaneous targeting of these factors (experimental condition, Figure 7A) resulted in a significant increase in the number of *tcf21*:H2B-Dendra2^{+} cells at 7dpi (Figures 7B–7E) in the injury area (arrowheads in Figures 7B′–7E′, quantification in Figure 7F, median control: 2.02 per 1,000 μm^2, n = 7; median experimental: 4.58 per 1,000 μm^2, n = 5; *p = 0.047) and also in non-injured regions of the ventricle (Figure 7G, median control: 0.2 per 1,000 μm^2, n = 7; median experimental: 0.34 per 1,000 μm^2, n = 5; **p = 0.004). This was accompanied by a reduction in the number of *hif1ab*, *nrf1*, *tbx2b*, and *zbtb7a* transcripts in the epicardial layer of loss-of-function hearts (Figures S6D–S6G), possibly due to the introduction of premature termination codons into the edited genes and activation of the nonsense-mediated mRNA decay pathway.[61] To assess proliferation, we stained against proliferating cell nuclear antigen (PCNA) and found a trend toward higher proliferation of *tcf21*:H2B-Dendra2^{+} cells in the wound area of loss-of-function hearts at 7 dpi (Figures S7A–S7C).

Focusing on the clearance of fibrotic tissue as an indicator of successful heart regeneration, we found that targeting *hif1ab*, *nrf1*, *tbx2b*, and *zbtb7a* impaired the resolution of fibrotic tissue at 22 dpi (Figures 7H and 7I, quantification in Figure 7J, median control: 1.97% ventricle area, n = 5; median experimental: 2.83% ventricle area, n = 7; *p = 0.028). At the same time, we noticed an increase in the thickness of the compact muscle layer covering the fibrotic tissue area (brackets in Figures 7H′ and 7I′, quantification in Figure 7K, median control: 42.25 μm, n = 5; median experimental: 70.43 μm, n = 7; *p = 0.015). The excess of fibrotic tissue after cryoinjury upon Cas9-mediated targeting of *hif1ab*, *nrf1*, *tbx2b*, and *zbtb7a*, in combination with the increase in epicardial cell numbers, strongly indicates that the epicardial regulatory core identified *in silico* has functional importance during zebrafish heart regeneration.

DISCUSSION

The epicardium is an essential source of cardiovascular derivatives and mitogenic signals during heart development and regeneration. Therefore, understanding the underlying genetic programs orchestrating epicardial development and response to injury is critical for successful therapeutic manipulation of the diseased heart.

It is generally accepted that the transcriptional programs employed during embryonic development are often repurposed during regeneration; yet, the genetic mechanisms underlying such programs remain elusive. In this study, we performed an unbiased genome-wide comparison of the epicardial gene programs acting during zebrafish epicardial development and following adult heart injury. Surprisingly, we found that the transcriptomic programs deployed during regeneration are not a mere recapitulation of the transcriptional activity driving embryonic development. By combining chromatin accessibility and gene expression data analysis, we built gene regulatory circuits that specifically govern each of these processes. We identified Wt1a, Wt1b, Klf9, and the AP-1 subunits Junbb, Fosab, and Fosb as more central in the developing epicardial gene regulatory network, suggesting that they may be required to activate the embryonic epicardial transcriptional program. Conversely, the regenerating epicardial gene regulatory network featured TFs such as Hif1ab, Zbtb7a, Tbx2b and Nrf1 as putative central regulators, with Hif1ab predicted to reside at the top of the regulatory hierarchy in the cryoinjured epicardium. We also found evidence that even for the group of transcripts shared by the embryonic and the regenerating epicardia, the underlying genetic programs driving their expression are distinct. Notably,

(C) TF motifs within the *mdka_e1* sequence.
(D) TF motifs within the *mdka_e2* sequence. Representative accessibility of the endogenous genomic region in *tcf21* larval epi (C) or in *tcf21* cryo (D) is underlaid in gray. Bubble size indicates the eigenvector centrality of the factor in the *tcf21* larval epi sub-network (C) or the *tcf21* cryo sub-network (D).
(E) mRNA staining of *klf9* (magenta) and *tcf21* (green) in a 5-dpf heart. (E′ and E′′) A nucleus (asterisk) in the epicardial region surrounded by *klf9* and *tcf21* transcripts.
(F) mRNA staining of *tbx2b* (magenta) and *tcf21* (green) in a 3-dpi cryoinjured adult heart. Ia, injury area. (F′ and F′′) A single nucleus (asterisk) in the epicardial region surrounded by *tbx2b* and *tcf21* transcripts.
(G) Predicted upstream transcriptional regulation in the developing epicardium.
(H) Upstream regulation in the regenerating epicardium.
In (G) and (H), all interactions are activating. Scale bars: 100 μm in (F); 20 μm in (E); and 5 μm in (E′), (E′′), (F′), and (F′′). Color channels have been adjusted separately for brightness/contrast. (E) and (F) are single optical sections. TFBS, transcription factor binding sites; V, ventricle. See also Figure S5.

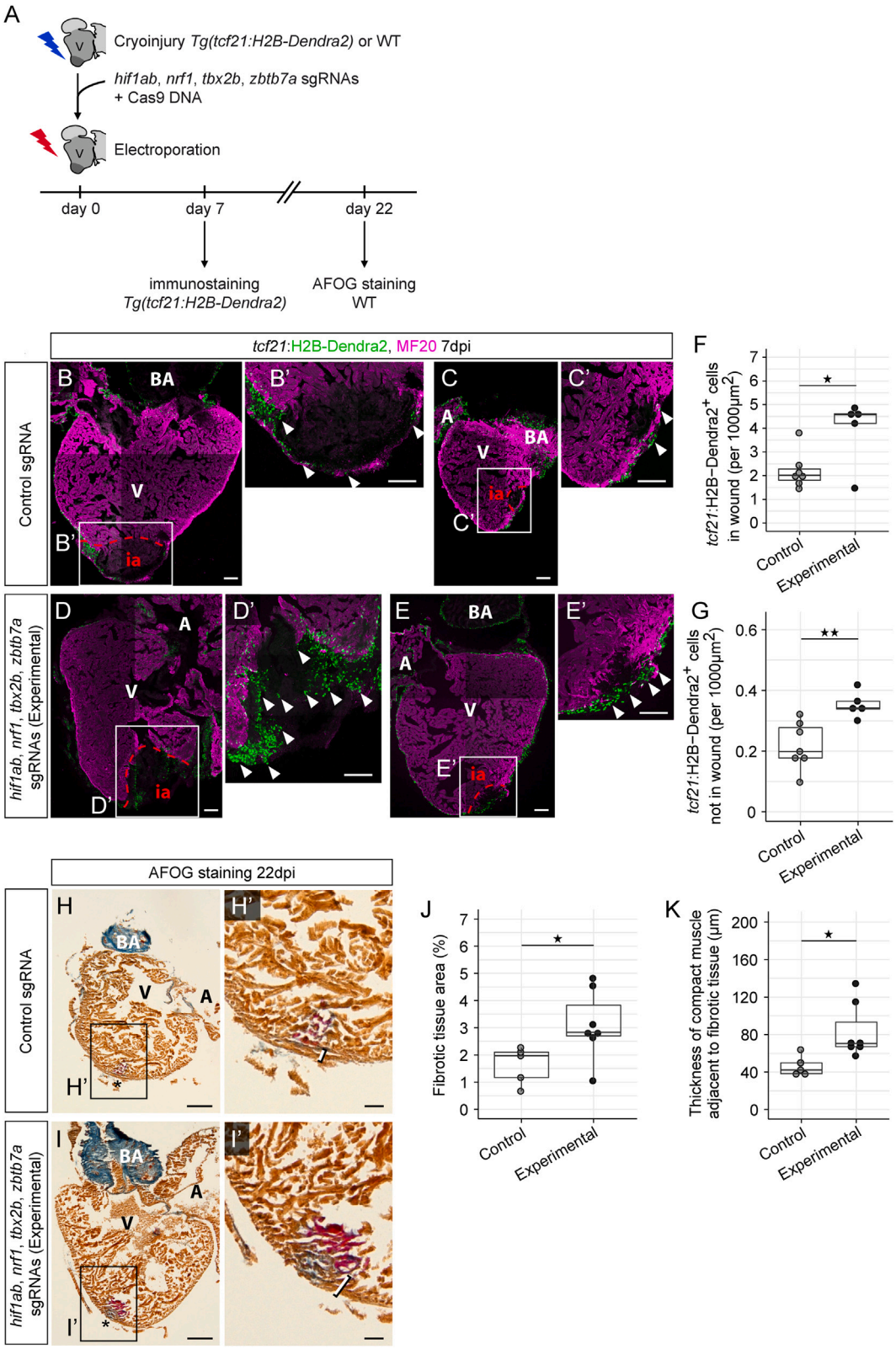

Figure 7. Loss of *hif1ab*, *nrf1*, *tbx2b*, and *zbtb7a* affects zebrafish heart regeneration

(A) Workflow of adult zebrafish heart injury followed by electroporation of a Cas9 expression vector and a mix of *hif1ab*, *nrf1*, *tbx2b*, and *zbtb7a* sgRNAs (experimental condition) or a control sgRNA.

(legend continued on next page)

Tcf21 positioning in each of the networks was strikingly different: while residing at the top of the developing TF hierarchy, Tcf21 received regulatory input from multiple sources, including itself, in the regenerating epicardial network. This suggests that the regulation of *tcf21* expression in the regenerating epicardium allows for multiple upstream inputs, which can potentially facilitate a rapid onset of expression upon injury, contrasting to the slower genomic regulatory blueprint deployed during development.

We validated the functional importance of a putative regulatory core acting in the regenerating epicardium, consisting of Hif1ab, Nrf1, Tbx2b, and Zbtb7a, via electroporation-based Cas9-mediated gene editing. Targeting *hif1ab*, *nrf1*, *tbx2b*, and *zbtb7a* at the time of cryoinjury resulted in increased epicardial cell numbers infiltrating the wound area and excess fibrosis. The loss of HIF-1a has recently been shown to increase mitochondrial reactive oxygen species (ROS) production in mouse cardiac fibroblasts after myocardial infarction, resulting in elevated fibroblast proliferation and excessive fibrosis.[62] Epicardial cells expressing *tcf21* are precursors of cardiac fibroblasts.[63] We indeed found that GO terms related to ROS, such as "response to reactive oxygen species" were over-represented ($p = 0.015$) in top Hif1ab target genes in the *tcf21* cryo network (connection probability > 0.995) (Figure S7D). A possible explanation for the increase in *tcf21*$^+$ cell numbers in the mutants is that the loss of *hif1ab* caused elevated ROS production in these cells, promoting proliferation within the epicardium. Indeed, we found a trend toward higher epicardial proliferation in the wound in mutant hearts at 7 dpi, albeit not significant. Because zebrafish epicardial cells are known to proliferate strongly at 3 dpi,[3,6] it is possible that the majority of *tcf21*$^+$ cells in the mutant hearts were generated via proliferation that took place before 7 dpi. That said, we cannot exclude at this stage that other mechanisms, such as an increased epithelial-to-mesenchymal transition (EMT) of epicardial cells, might contribute to the elevated *tcf21*$^+$ cell numbers in the wound.

Interestingly, ROS production in fibroblasts is induced by transforming growth factor β (TGF-β) signaling,[64,65] and it has recently been reported that NRF1 negatively regulates TGF-β in a mouse model of pulmonary fibrosis.[66] Indeed, the connection strength between Nrf1 and the TGF-β repressor Smad7 in the *tcf21* cryo network (probability = 0.96) was comparable to that of the connections between Nrf1 and known Nrf1 targets such as Tfam[67] (probability = 0.94) and Tfb2m[68] (probability = 0.99). In the injured zebrafish heart, the TGF-β ligand *tgfb1* is expressed in epicardial cells and fibroblasts, and TGF-β signaling mediates fibrotic tissue deposition in the wound.[22] It is plausible that the loss of *nrf1* led to an over-activation of TGF-β signaling in *tcf21*$^+$ cardiac cells after cryoinjury, causing the excess fibrosis observed in the mutant hearts. In addition, the higher number of *tcf21*$^+$ cells in the experimental condition alone is likely to have increased fibrotic tissue deposition in the wound area because we found collagens and several other ECM constituents, such as *fn1a*, expressed in cardiac *tcf21*$^+$ cells after cryoinjury.

The increase in *tcf21*$^+$ cells may also explain the thickened compact muscle layer covering the wound area in the mutants at 22 dpi. Epicardial cells act as a signaling hub following cardiac injury, stimulating cardiomyocyte proliferation via paracrine factors such as retinoic acid[13] and neuregulin 1.[69] Upon cardiac injury, the epicardium also produces the chemokine Cxcl12a, which directs the migration of cardiomyocytes into the wound area.[70] Further studies are required to determine whether the increase in the number of epicardial cells leads to elevated mitogenic signaling and enhanced cardiomyocyte proliferation and migration in the setting of heart injury and regeneration.

Our work undertakes a genome-wide approach based on epicardial gene expression and chromatin accessibility profiles to build, compare, and contrast gene regulatory networks specifically driving epicardial genetic programs during embryonic development and regeneration. Here, we provide insights into the differential regulation of each of these processes and propose that the slower process of epicardial development involves a pre-planned series of coordinated events. In contrast, injury and regeneration entail a rapid response mode. Consequently, the positioning, utilization, and occupancy of regulatory elements are different in each of these processes. A deep understanding of the gene regulatory mechanisms underlying dynamic changes in epicardial gene expression is key to potentially developing therapeutics that can induce regeneration of the non-regenerative mammalian heart.

Limitations of the study

When generating our transcriptomic dataset, we applied fluorescence-activated cell sorting (FACS) to isolate larval epicardial cells and biotagging pull-down to isolate adult epicardial cell nuclei. This was due to technical reasons, i.e. low larval epicardial cell numbers leading to limited material for nuclear pull-down and adult epicardial cells being adversely affected during the sorting. We note the potential for additional variability introduced by cell versus nuclei isolation. However, the identification

(B–E) Control (B and C) and experimental (D and E) *TgBAC(tcf21:H2B-Dendra2)* hearts at 7 dpi, stained against Dendra2 (green) and MF20 (magenta). Shown are hearts with large injuries (B and D) and small injuries (C and E). (B′–E′) show magnifications of the injury areas in (B)–(E), respectively. Arrowheads indicate epicardial cells in the injury area.

(F) Quantification of *tcf21*$^+$ cardiac cell numbers in the injury area (*$p = 0.047$).

(G) Quantification of *tcf21*$^+$ cardiac cell numbers in the non-injury area of the ventricle (**$p = 0.004$). Cell numbers in (F) and (G) have been normalized against injury area (F) and non-injury ventricle area (G). In (F) and (G): n(control) = 7, n(experimental) = 5.

(H and I) Acid Fuchsin Orange-G (AFOG) staining showing healthy tissue (orange-brown), fibrin (red), and collagen (blue) in control (H) and experimental (I) hearts at 22 dpi. Asterisks indicate the site of injury. (H′) and (I′) show magnifications of the injury areas in (H) and (I), respectively. Brackets indicate the thickness of the compact muscle layer at the injury site.

(J) Quantification of AFOG-stained tissue areas, normalized against ventricle area (*$p = 0.028$).

(K) Quantification of the thickness of the compact muscle layer at the injury site (*$p = 0.015$).

In (J) and (K): n(control) = 5, n(experimental) = 7. Scale bars: 100 μm in (B)–(E) and (B′)–(E′), 200 μm in (H) and (I), and 50 μm in (H′) and (I′). A, atrium; BA, bulbus arteriosus; V, ventricle; WT, wild type; ia, injury area. In (F), (G), (J) and (K), box and whiskers plots (in the style of Tukey) indicate median and first/third quartiles. See also Figures S6 and S7 and Table S3.

of genes common to developing and regenerating epicardia will not have been affected because we performed differential gene expression analyses only between the larval conditions, as well as between the adult conditions, and did not perform a direct statistical comparison between larval and adult epicardium. Moreover, although possible technical variations might have affected the gene regulatory networks that we constructed, we validated the expression of several central regulators in these networks via HCR, which matched our computational analysis.

STAR★METHODS

Detailed methods are provided in the online version of this paper and include the following:

- KEY RESOURCES TABLE
- RESOURCE AVAILABILITY
  - Lead contact
  - Materials availability
  - Data and code availability
- EXPERIMENTAL MODEL AND STUDY PARTICIPANT DETAILS
  - Zebrafish Lines
  - Generation of transgenic zebrafish lines
- METHOD DETAILS
  - Hybridisation Chain Reaction
  - Immunocytochemistry
  - Histology
  - Larval heart Isolation, Dissociation and FAC-Sorting
  - Adult zebrafish heart injury
  - Biotagged nuclei isolation
  - RNA extraction and library preparation for sequencing
  - ATAC Sequencing
  - Electroporation of enhancer reporter constructs into the adult zebrafish heart
- QUANTIFICATION AND STATISTICAL ANALYSIS
  - Published Datasets
  - RNA Sequencing Data Analysis
  - ATAC Sequencing Data Analysis
  - Transcription Factor Binding Site Analysis
  - Gene Regulatory Networks

SUPPLEMENTAL INFORMATION

Supplemental information can be found online at https://doi.org/10.1016/j.devcel.2023.12.012.

ACKNOWLEDGMENTS

We would like to thank the Biomedical Services Unit for fish husbandry, as well as MRC WIMM Flow Cytometry Facility, MRC WIMM Sequencing Facility, MRC WIMM Single Cell Core Facility, and the Wolfson Imaging Centre Oxford for excellent services. We are grateful to Richard White and Yilun Ma for providing us with the *ubb*:Cas9 and *CMV*:Tol2 plasmids. We thank Seda Ates and Jasmina Kuburic for technical assistance. This work was supported by BHF grants RG/13/9/303269 and CH/11/1/28798 to P.R.R. and M.W., BHF Research Fellowship FS/IBSRF/21/25088 and Oxford BHF Centre of Research Excellence fellowship RE/13/1/30181 award to F.C.S. and T.G., and Wellcome Trust Senior Research Fellowship (215615/Z/19/Z) to T.S.-S.

AUTHOR CONTRIBUTIONS

Conceptualization, M.W., F.C.S., T.S.-S., and P.R.R.; methodology, M.W., F.C.S., and T.G.; investigation, M.W., F.C.S., and T.G.; computational analysis and data curation, M.W.; writing – original draft, M.W. and F.C.S.; writing – review & editing, M.W., F.C.S., T.S.-S., and P.R.R.; supervision, T.S.-S. and P.R.R.; funding acquisition, T.S.-S. and P.R.R.

DECLARATION OF INTERESTS

The authors declare no competing interests.

Received: August 5, 2022
Revised: August 12, 2023
Accepted: December 20, 2023
Published: January 17, 2024

REFERENCES

1. Haubner, B.J., Schneider, J., Schweigmann, U., Schuetz, T., Dichtl, W., Velik-Salchner, C., Stein, J.I., and Penninger, J.M. (2016). Functional recovery of a human neonatal heart after severe myocardial infarction. Circ. Res. *118*, 216–221.
2. Porrello, E.R., Mahmoud, A.I., Simpson, E., Hill, J.A., Richardson, J.A., Olson, E.N., and Sadek, H.A. (2011). Transient regenerative potential of the neonatal mouse heart. Science *331*, 1078–1080.
3. González-Rosa, J.M., Martín, V., Peralta, M., Torres, M., and Mercader, N. (2011). Extensive scar formation and regression during heart regeneration after cryoinjury in zebrafish. Development *138*, 1663–1674.
4. Poss, K.D., Wilson, L.G., and Keating, M.T. (2002). Heart regeneration in zebrafish. Science *298*, 2188–2190.
5. Chablais, F., Veit, J., Rainer, G., and Jaźwińska, A. (2011). The zebrafish heart regenerates after cryoinjury-induced myocardial infarction. BMC Dev. Biol. *11*, 21.
6. Schnabel, K., Wu, C.C., Kurth, T., and Weidinger, G. (2011). Regeneration of cryoinjury induced necrotic heart lesions in zebrafish is associated with epicardial activation and cardiomyocyte proliferation. PLoS One *6*, e18503.
7. Foglia, M.J., and Poss, K.D. (2016). Building and re-building the heart by cardiomyocyte proliferation. Development *143*, 729–740.
8. González-Rosa, J.M., Burns, C.E., and Burns, C.G. (2017). Zebrafish heart regeneration: 15 years of discoveries. Regeneration (Oxf.) *4*, 105–123.
9. Simões, F.C., and Riley, P.R. (2018). The ontogeny, activation and function of the epicardium during heart development and regeneration. Development *145*, dev155994.
10. Wang, J., Cao, J., Dickson, A.L., and Poss, K.D. (2015). Epicardial regeneration is guided by cardiac outflow tract and Hedgehog signalling. Nature *522*, 226–230.
11. González-Rosa, J.M., Peralta, M., and Mercader, N. (2012). Pan-epicardial lineage tracing reveals that epicardium derived cells give rise to myofibroblasts and perivascular cells during zebrafish heart regeneration. Dev. Biol. *370*, 173–186.
12. Kikuchi, K., Gupta, V., Wang, J., Holdway, J.E., Wills, A.A., Fang, Y., and Poss, K.D. (2011). tcf21+ epicardial cells adopt non-myocardial fates during zebrafish heart development and regeneration. Development *138*, 2895–2902.
13. Kikuchi, K., Holdway, J.E., Major, R.J., Blum, N., Dahn, R.D., Begemann, G., and Poss, K.D. (2011). Retinoic acid production by endocardium and epicardium is an injury response essential for zebrafish heart regeneration. Dev. Cell *20*, 397–404.
14. Lepilina, A., Coon, A.N., Kikuchi, K., Holdway, J.E., Roberts, R.W., Burns, C.G., and Poss, K.D. (2006). A dynamic epicardial injury response supports progenitor cell activity during zebrafish heart regeneration. Cell *127*, 607–619.
15. Marro, J., Pfefferli, C., de Preux Charles, A.S., Bise, T., and Jaźwińska, A. (2016). Collagen XII contributes to epicardial and connective tissues in the

zebrafish heart during ontogenesis and regeneration. PLoS One *11*, e0165497.

16. Mercer, S.E., Odelberg, S.J., and Simon, H.G. (2013). A dynamic spatiotemporal extracellular matrix facilitates epicardial-mediated vertebrate heart regeneration. Dev. Biol. *382*, 457–469.
17. Wang, J., Karra, R., Dickson, A.L., and Poss, K.D. (2013). Fibronectin is deposited by injury-activated epicardial cells and is necessary for zebrafish heart regeneration. Dev. Biol. *382*, 427–435.
18. Choi, W.Y., Gemberling, M., Wang, J., Holdway, J.E., Shen, M.C., Karlstrom, R.O., and Poss, K.D. (2013). In vivo monitoring of cardiomyocyte proliferation to identify chemical modifiers of heart regeneration. Development *140*, 660–666.
19. Sugimoto, K., Hui, S.P., Sheng, D.Z., and Kikuchi, K. (2017). Dissection of zebrafish shha function using site-specific targeting with a Cre-dependent genetic switch. Elife *6*, e24635.
20. Huang, Y., Harrison, M.R., Osorio, A., Kim, J., Baugh, A., Duan, C., Sucov, H.M., and Lien, C.L. (2013). Igf signaling is required for cardiomyocyte proliferation during zebrafish heart development and regeneration. PLoS One *8*, e67266.
21. Wu, C.C., Kruse, F., Vasudevarao, M.D., Junker, J.P., Zebrowski, D.C., Fischer, K., Noël, E.S., Grün, D., Berezikov, E., Engel, F.B., et al. (2016). Spatially resolved genome-wide transcriptional profiling identifies BMP signaling as essential regulator of zebrafish cardiomyocyte regeneration. Dev. Cell *36*, 36–49.
22. Chablais, F., and Jazwinska, A. (2012). The regenerative capacity of the zebrafish heart is dependent on TGFbeta signaling. Development *139*, 1921–1930.
23. Goldman, J.A., and Poss, K.D. (2020). Gene regulatory programmes of tissue regeneration. Nat. Rev. Genet. *21*, 511–525.
24. Wang, Z., Cui, M., Shah, A.M., Tan, W., Liu, N., Bassel-Duby, R., and Olson, E.N. (2020). Cell-type-specific gene regulatory networks underlying murine neonatal heart regeneration at single-cell resolution. Cell Rep. *33*, 108472.
25. Wang, Z., Cui, M., Shah, A.M., Ye, W., Tan, W., Min, Y.L., Botten, G.A., Shelton, J.M., Liu, N., Bassel-Duby, R., and Olson, E.N. (2019). Mechanistic basis of neonatal heart regeneration revealed by transcriptome and histone modification profiling. Proc. Natl. Acad. Sci. USA *116*, 18455–18465.
26. Bollini, S., Vieira, J.M., Howard, S., Dubè, K.N., Balmer, G.M., Smart, N., and Riley, P.R. (2014). Re-activated adult epicardial progenitor cells are a heterogeneous population molecularly distinct from their embryonic counterparts. Stem Cells Dev. *23*, 1719–1730.
27. Long, H.K., Prescott, S.L., and Wysocka, J. (2016). Ever-changing landscapes: transcriptional enhancers in development and evolution. Cell *167*, 1170–1187.
28. Felsenfeld, G., and Groudine, M. (2003). Controlling the double helix. Nature *421*, 448–453.
29. Buenrostro, J.D., Giresi, P.G., Zaba, L.C., Chang, H.Y., and Greenleaf, W.J. (2013). Transposition of native chromatin for fast and sensitive epigenomic profiling of open chromatin, DNA-binding proteins and nucleosome position. Nat. Methods *10*, 1213–1218.
30. Pfefferli, C., and Jaźwińska, A. (2017). The careg element reveals a common regulation of regeneration in the zebrafish myocardium and fin. Nat. Commun. *8*, 15151.
31. Wang, W., Hu, C.K., Zeng, A., Alegre, D., Hu, D., Gotting, K., Ortega Granillo, A., Wang, Y., Robb, S., Schnittker, R., et al. (2020). Changes in regeneration-responsive enhancers shape regenerative capacities in vertebrates. Science *369*, eaaz3090.
32. Begeman, I.J., Shin, K., Osorio-Méndez, D., Kurth, A., Lee, N., Chamberlain, T.J., Pelegri, F.J., and Kang, J. (2020). Decoding an organ regeneration switch by dissecting cardiac regeneration enhancers. Development *147*, dev194019.
33. Kang, J., Hu, J., Karra, R., Dickson, A.L., Tornini, V.A., Nachtrab, G., Gemberling, M., Goldman, J.A., Black, B.L., and Poss, K.D. (2016). Modulation of tissue repair by regeneration enhancer elements. Nature *532*, 201–206.
34. Goldman, J.A., Kuzu, G., Lee, N., Karasik, J., Gemberling, M., Foglia, M.J., Karra, R., Dickson, A.L., Sun, F., Tolstorukov, M.Y., and Poss, K.D. (2017). Resolving heart regeneration by replacement histone profiling. Dev. Cell *40*, 392–404.e5.
35. Huang, G.N., Thatcher, J.E., McAnally, J., Kong, Y., Qi, X., Tan, W., DiMaio, J.M., Amatruda, J.F., Gerard, R.D., Hill, J.A., et al. (2012). C/EBP transcription factors mediate epicardial activation during heart development and injury. Science *338*, 1599–1603.
36. Vieira, J.M., Howard, S., Villa Del Campo, C., Bollini, S., Dubé, K.N., Masters, M., Barnette, D.N., Rohling, M., Sun, X., Hankins, L.E., et al. (2017). BRG1-SWI/SNF-dependent regulation of the Wt1 transcriptional landscape mediates epicardial activity during heart development and disease. Nat. Commun. *8*, 16034.
37. Cao, Y., Xia, Y., Balowski, J.J., Ou, J., Song, L., Safi, A., Curtis, T., Crawford, G.E., Poss, K.D., and Cao, J. (2022). Identification of enhancer regulatory elements that direct epicardial gene expression during zebrafish heart regeneration. Development *149*, dev200133.
38. Simões, F.C., Cahill, T.J., Kenyon, A., Gavriouchkina, D., Vieira, J.M., Sun, X., Pezzolla, D., Ravaud, C., Masmanian, E., Weinberger, M., et al. (2020). Macrophages directly contribute collagen to scar formation during zebrafish heart regeneration and mouse heart repair. Nat. Commun. *11*, 600.
39. Trinh, L.A., Chong-Morrison, V., Gavriouchkina, D., Hochgreb-Hägele, T., Senanayake, U., Fraser, S.E., and Sauka-Spengler, T. (2017). Biotagging of specific cell populations in zebrafish reveals gene regulatory logic encoded in the nuclear transcriptome. Cell Rep. *19*, 425–440.
40. Grivas, D., González-Rajal, Á., and de la Pompa, J.L. (2021). Midkine-a regulates the formation of a fibrotic scar during zebrafish heart regeneration. Front. Cell Dev. Biol. *9*, 669439.
41. Sánchez-Iranzo, H., Galardi-Castilla, M., Sanz-Morejón, A., González-Rosa, J.M., Costa, R., Ernst, A., Sainz de Aja, J., Langa, X., and Mercader, N. (2018). Transient fibrosis resolves via fibroblast inactivation in the regenerating zebrafish heart. Proc. Natl. Acad. Sci. USA *115*, 4188–4193.
42. Björkblom, B., Padzik, A., Mohammad, H., Westerlund, N., Komulainen, E., Hollos, P., Parviainen, L., Papageorgiou, A.C., Iljin, K., Kallioniemi, O., et al. (2012). C-Jun N-terminal kinase phosphorylation of MARCKSL1 determines actin stability and migration in neurons and in cancer cells. Mol. Cell. Biol. *32*, 3513–3526.
43. van der Slot, A.J., Zuurmond, A.M., Bardoel, A.F., Wijmenga, C., Pruijs, H.E., Sillence, D.O., Brinckmann, J., Abraham, D.J., Black, C.M., Verzijl, N., et al. (2003). Identification of PLOD2 as telopeptide lysyl hydroxylase, an important enzyme in fibrosis. J. Biol. Chem. *278*, 40967–40972.
44. Choi, H.M.T., Schwarzkopf, M., Fornace, M.E., Acharya, A., Artavanis, G., Stegmaier, J., Cunha, A., and Pierce, N.A. (2018). Third-generation in situ hybridization chain reaction: multiplexed, quantitative, sensitive, versatile, robust. Development *145*, dev165753.
45. Zhang, Y., Liu, T., Meyer, C.A., Eeckhoute, J., Johnson, D.S., Bernstein, B.E., Nusbaum, C., Myers, R.M., Brown, M., Li, W., and Liu, X.S. (2008). Model-based analysis of ChIP-Seq (MACS). Genome Biol. *9*, R137.
46. Stark, R., and Brown, G. (2011). DiffBind: Differential Binding Analysis of ChIP-Seq Peak Data. https://bioconductor.org/packages/release/bioc/vignettes/DiffBind/inst/doc/DiffBind.pdf.
47. Heinz, S., Benner, C., Spann, N., Bertolino, E., Lin, Y.C., Laslo, P., Cheng, J.X., Murre, C., Singh, H., and Glass, C.K. (2010). Simple combinations of lineage-determining transcription factors prime cis-regulatory elements required for macrophage and B cell identities. Mol. Cell *38*, 576–589.
48. Melodelima, C., and Gautier, C. (2008). The GC-heterogeneity of teleost fishes. BMC Genomics *9*, 632.
49. Illingworth, R.S., Gruenewald-Schneider, U., Webb, S., Kerr, A.R., James, K.D., Turner, D.J., Smith, C., Harrison, D.J., Andrews, R., and Bird, A.P. (2010). Orphan CpG islands identify numerous conserved promoters in the mammalian genome. PLoS Genet. *6*, e1001134.

50. Chong-Morrison, V., Mayes, S., Simões, F.C., Senanayake, U., Carroll, D.S., Riley, P.R., Wilson, S.W., and Sauka-Spengler, T. (2023). Ac/Ds transposition for CRISPR/dCas9-SID4x epigenome modulation in zebrafish. Biol. Open *12*, bio059995.

51. Callahan, S.J., Tepan, S., Zhang, Y.M., Lindsay, H., Burger, A., Campbell, N.R., Kim, I.S., Hollmann, T.J., Studer, L., Mosimann, C., and White, R.M. (2018). Cancer modeling by Transgene Electroporation in Adult Zebrafish (TEAZ). Dis. Model. Mech. *11*, dmm034561.

52. Fornes, O., Castro-Mondragon, J.A., Khan, A., van der Lee, R., Zhang, X., Richmond, P.A., Modi, B.P., Correard, S., Gheorghe, M., Baranašić, D., et al. (2020). JASPAR 2020: update of the open-access database of transcription factor binding profiles. Nucleic Acids Res. *48*, D87–D92.

53. Schep, A.N., Wu, B., Buenrostro, J.D., and Greenleaf, W.J. (2017). chromVAR: inferring transcription-factor-associated accessibility from single-cell epigenomic data. Nat. Methods *14*, 975–978.

54. Beisaw, A., Kuenne, C., Guenther, S., Dallmann, J., Wu, C.C., Bentsen, M., Looso, M., and Stainier, D.Y.R. (2020). AP-1 contributes to chromatin accessibility to promote sarcomere disassembly and cardiomyocyte protrusion during zebrafish heart regeneration. Circ. Res. *126*, 1760–1778.

55. Sun, J., Peterson, E.A., Wang, A.Z., Ou, J., Smith, K.E., Poss, K.D., and Wang, J. (2022). hapln1 defines an epicardial cell subpopulation required for cardiomyocyte expansion during heart morphogenesis and regeneration. Circulation *146*, 48–63.

56. Jopling, C., Suñé, G., Faucherre, A., Fabregat, C., and Izpisua Belmonte, J.C. (2012). Hypoxia induces myocardial regeneration in zebrafish. Circulation *126*, 3017–3027.

57. Niu, X., Zhang, J., Zhang, L., Hou, Y., Pu, S., Chu, A., Bai, M., and Zhang, Z. (2019). Weighted gene co-expression network analysis identifies critical genes in the development of heart failure after acute myocardial infarction. Front. Genet. *10*, 1214.

58. Chi, N.C., Shaw, R.M., De Val, S., Kang, G., Jan, L.Y., Black, B.L., and Stainier, D.Y. (2008). Foxn4 directly regulates tbx2b expression and atrioventricular canal formation. Genes Dev. *22*, 734–739.

59. Xu, Q., Georgiou, G., Frölich, S., van der Sande, M., Veenstra, G.J.C., Zhou, H., and van Heeringen, S.J. (2021). ANANSE: an enhancer network-based computational approach for predicting key transcription factors in cell fate determination. Nucleic Acids Res. *49*, 7966–7985.

60. Csardi, G., and Nepusz, T. (2006). The igraph software package for complex network research. InterJournal, Complex Systems *1695*, 1–9.

61. Kurosaki, T., Popp, M.W., and Maquat, L.E. (2019). Quality and quantity control of gene expression by nonsense-mediated mRNA decay. Nat. Rev. Mol. Cell Biol. *20*, 406–420.

62. Janbandhu, V., Tallapragada, V., Patrick, R., Li, Y., Abeygunawardena, D., Humphreys, D.T., Martin, E.M.M.A., Ward, A.O., Contreras, O., Farbehi, N., et al. (2022). Hif-1a suppresses ROS-induced proliferation of cardiac fibroblasts following myocardial infarction. Cell Stem Cell *29*, 281–297.e12.

63. Xia, Y., Duca, S., Perder, B., Dündar, F., Zumbo, P., Qiu, M., Yao, J., Cao, Y., Harrison, M.R.M., Zangi, L., et al. (2022). Activation of a transient progenitor state in the epicardium is required for zebrafish heart regeneration. Nat. Commun. *13*, 7704.

64. Jain, M., Rivera, S., Monclus, E.A., Synenki, L., Zirk, A., Eisenbart, J., Feghali-Bostwick, C., Mutlu, G.M., Budinger, G.R., and Chandel, N.S. (2013). Mitochondrial reactive oxygen species regulate transforming growth factor-beta signaling. J. Biol. Chem. *288*, 770–777.

65. Thannickal, V.J., and Fanburg, B.L. (1995). Activation of an H2O2-generating NADH oxidase in human lung fibroblasts by transforming growth factor beta 1. J. Biol. Chem. *270*, 30334–30338.

66. Suliman, H.B., Healy, Z., Zobi, F., Kraft, B.D., Welty-Wolf, K., Smith, J., Barkauskas, C., and Piantadosi, C.A. (2022). Nuclear respiratory factor-1 negatively regulates TGF-beta1 and attenuates pulmonary fibrosis. iScience *25*, 103535.

67. Scarpulla, R.C. (2006). Nuclear control of respiratory gene expression in mammalian cells. J. Cell. Biochem. *97*, 673–683.

68. Gleyzer, N., Vercauteren, K., and Scarpulla, R.C. (2005). Control of mitochondrial transcription specificity factors (TFB1M and TFB2M) by nuclear respiratory factors (NRF-1 and NRF-2) and PGC-1 family coactivators. Mol. Cell. Biol. *25*, 1354–1366.

69. Gemberling, M., Karra, R., Dickson, A.L., and Poss, K.D. (2015). Nrg1 is an injury-induced cardiomyocyte mitogen for the endogenous heart regeneration program in zebrafish. Elife *4*, e05871.

70. Itou, J., Oishi, I., Kawakami, H., Glass, T.J., Richter, J., Johnson, A., Lund, T.C., and Kawakami, Y. (2012). Migration of cardiomyocytes is essential for heart regeneration in zebrafish. Development *139*, 4133–4142.

71. Weinberger, M., Simões, F.C., Patient, R., Sauka-Spengler, T., and Riley, P.R. (2020). Functional heterogeneity within the developing zebrafish epicardium. Dev. Cell *52*, 574–590.e6.

72. Dobin, A., Davis, C.A., Schlesinger, F., Drenkow, J., Zaleski, C., Jha, S., Batut, P., Chaisson, M., and Gingeras, T.R. (2013). STAR: ultrafast universal RNA-seq aligner. Bioinformatics *29*, 15–21.

73. Langmead, B., Trapnell, C., Pop, M., and Salzberg, S.L. (2009). Ultrafast and memory-efficient alignment of short DNA sequences to the human genome. Genome Biol. *10*, R25.

74. Li, H., Handsaker, B., Wysoker, A., Fennell, T., Ruan, J., Homer, N., Marth, G., Abecasis, G., and Durbin, R.; 1000 Genome Project Data Processing Subgroup (2009). The Sequence Alignment/Map format and SAMtools. Bioinformatics *25*, 2078–2079.

75. Liao, Y., Smyth, G.K., and Shi, W. (2014). featureCounts: an efficient general purpose program for assigning sequence reads to genomic features. Bioinformatics *30*, 923–930.

76. Love, M.I., Huber, W., and Anders, S. (2014). Moderated estimation of fold change and dispersion for RNA-seq data with DESeq2. Genome Biol. *15*, 550.

77. Robinson, M.D., McCarthy, D.J., and Smyth, G.K. (2010). edgeR: a Bioconductor package for differential expression analysis of digital gene expression data. Bioinformatics *26*, 139–140.

78. Alexa, A., and Rahnenfuhrer, J. (2021). topGO: Enrichment Analysis for Gene Ontology. Bioconductor).

79. van Heeringen, S.J., and Veenstra, G.J. (2011). GimmeMotifs: a de novo motif prediction pipeline for ChIP-sequencing experiments. Bioinformatics *27*, 270–271.

80. Longabaugh, W.J., Davidson, E.H., and Bolouri, H. (2005). Computational representation of developmental genetic regulatory networks. Dev. Biol. *283*, 1–16.

81. Bussmann, J., and Schulte-Merker, S. (2011). Rapid BAC selection for tol2-mediated transgenesis in zebrafish. Development *138*, 4327–4332.

82. Chong-Morrison, V., Simões, F.C., Senanayake, U., Carroll, D.S., Riley, P.R., and Sauka-Spengler, T. (2018). Re-purposing Ac/Ds transgenic system for CRISPR/dCas9 modulation of enhancers and non-coding RNAs in zebrafish. Preprint at bioRxiv. https://doi.org/10.1101/450684.

83. Burns, C.G., and MacRae, C.A. (2006). Purification of hearts from zebrafish embryos. BioTechniques *40*, 276.

84. Wickham, H. (2016). Ggplot2: Elegant Graphics for Data Analysis (Springer-Verlag New York).

85. Kent, W.J., Sugnet, C.W., Furey, T.S., Roskin, K.M., Pringle, T.H., Zahler, A.M., and Haussler, D. (2002). The human genome browser at UCSC. Genome Res. *12*, 996–1006.

86. Kamimoto, K., Hoffmann, C.M., and Morris, S.A. (2020). CellOracle: dissecting cell identity via network inference and in silico gene perturbation. Preprint at bioRxiv. https://doi.org/10.1101/2020.02.17.947416.

STAR★METHODS

KEY RESOURCES TABLE

REAGENT or RESOURCE	SOURCE	IDENTIFIER
Antibodies		
chicken polyclonal anti-GFP	abcam	Cat# ab13970, RRID:AB_300798
Living Colors® DsRed Polyclonal Antibody rabbit	Clontech	Cat# 632496, RRID:AB_10013483
Dendra2 Polyclonal Antibody rabbit	Thermo Fisher Scientific	PA5-122326, RRID:AB_2915898
mouse IgG2b anti-MYH1E	DSHB	Cat# MF 20, RRID:AB_2147781
Anti-PCNA antibody [PC10] mouse	Abcam	Cat# ab29, RRID:AB_303394
Chemicals, peptides, and recombinant proteins		
Herculase II Fusion DNA Polymerase	Agilent	Cat# 600675
Antigen Unmasking Solution, Citric Acid Based	Vector Laboratories	H-3300
Critical commercial assays		
NextSeq ® 500/550 High Output Kit v2.5 (75 cycles)	Illumina	Cat# 20024906
NextSeq ® 500/550 High Output Kit v2.5 (150 cycles)	Illumina	Cat# 20024907
SMART-SeqTm v4 UltraTm Low Input RNA Kit for Sequencing	Clontech	Cat# 634888
Nextera XT library preparation kit	Illumina	Cat# FC-131-1024
InFusion HD Cloning kit	Clontech	Cat# 638910
See method details section for Hybridization Chain Reaction (HCR) v3.0	Molecular Instruments	N/A
Deposited data		
Custom code for an analysis pipeline of bulk ATAC-seq data	This Manuscript	Zenodo: https://doi.org/10.5281/zenodo.10384511
Bulk RNA-seq data and bulk ATAC-seq data	This Manuscript	GEO: GSE178751
RNA-seq data from intact adult zebrafish epicardium	See Sun et al.[55]	GEO: GSE172511
Experimental models: Organisms/strains		
TgBAC(tcf21:H2B-Dendra2)^{ox182}	See Weinberger et al.[71]	OX182
TgBAC(tcf21:myr-eGFP)^{ox183}	See Weinberger et al.[71]	OX183
Tg(βactin:Avi-Cerulean-RanGap)^{ct700a}	See Trinh et al.[39]	CT700a
TgBAC(tcf21:BirA-2a-mCherry)^{ox143}	This Manuscript	OX143
Tg(mdka_e1:mCherry)^{ox195}	This Manuscript	OX195
Tg(mdka_e2:mCherry)^{ox197}	This Manuscript	OX197
Tg(col12a1a_e1:mCherry)^{ox196}	This Manuscript	OX196
Oligonucleotides		
See Table S2 for enhancer amplification primers	This Manuscript	N/A
See Table S3 for sgRNA sequences	This Manuscript	N/A
Recombinant DNA		
pVC-Ds-mdka_e1-E1b:mCherry-Ds	This Manuscript	Addgene: Cat# 210384
pVC-Ds-mdka_e2-E1b:mCherry-Ds	This Manuscript	Addgene: Cat# 210385
pVC-Ds-col12a1a_e1-E1b:mCherry-Ds	This Manuscript	Addgene: Cat# 210386

(*Continued on next page*)

Continued

REAGENT or RESOURCE	SOURCE	IDENTIFIER
BAC clone DKEYP-79F12	https://www.sourcebioscience.com	DKEYP-79F12
pGEM-cytoBirA-2A-mCherry-SV40pA-FKF	See Trinh et al.[39]	Addgene: Cat# 79887
ubb:Cas9 plasmid containing Tol2 recognition sites	Richard White Lab	N/A
CMV:Tol2	Richard White Lab	N/A
Software and algorithms		
STAR v2.4.2a	See Dobin et al.[72]	https://github.com/alexdobin/STAR
bowtie v1.2.3	See Langmead et al.[73]	https://bowtie-bio.sourceforge.net/index.shtml
samtools v1.10	See Li et al.[74]	http://htslib.org/
FeatureCounts v1.6.2	See Liao et al.[75]	http://bioinf.wehi.edu.au/featureCounts
MACS v2.2.7.1	See Zhang et al.[45]	https://github.com/macs3-project/MACS
Homer v20201202	See Heinz et al.[47]	http://homer.ucsd.edu/homer/
R v4.0.3	R Core Team	https://www.r-project.org/
DESeq2 v1.30.0	See Love et al.[76]	https://bioconductor.org/packages/release/bioc/html/DESeq2.html
edgeR v3.32.1	See Robinson et al.[77]	https://bioconductor.org/packages/release/bioc/html/edgeR.html
topGO v2.42.1	See Alexa and Rahnenfuehrer[78]	http://bioconductor.org/packages/release/bioc/html/topGO.html
DiffBind v3.0.13	See Stark and Brown[46]	https://bioconductor.org/packages/release/bioc/html/DiffBind.html
gimmemotifs	See van Heeringen and Veenstra[79]	https://gimmemotifs.readthedocs.io/en/master/
JASPAR2020 v0.99.10	See Fornes et al.[52]	https://bioconductor.org/packages/release/data/annotation/html/JASPAR2020.html
chromVAR v1.12.0	See Schep et al.[53]	https://bioconductor.org/packages/release/bioc/html/chromVAR.html
Ananse v0.1.7	See Xu et al.[59]	https://anansepy.readthedocs.io/en/master/
BioTapestry v7.1.2.0	See Longabaugh et al.[80]	https://biotapestry.systemsbiology.net/

RESOURCE AVAILABILITY

Lead contact

Further information and requests for resources and reagents should be directed to and will be fulfilled by the lead contact, Paul Riley (paul.riley@idrm.ox.ac.uk).

Materials availability

Requests for zebrafish transgenic lines should be directed to Tatjana Sauka-Spengler (tatjana.sauka-spengler@imm.ox.ac.uk). Plasmids generated in this study have been submitted to Addgene (www.addgene.org/Tatjana_Sauka-Spengler/ pVC-Ds-mdka_e1-E1b:mCherry-Ds, Cat# 210384; pVC-Ds-mdka_e2-E1b:mCherry-Ds, Cat# 210385; pVC-Ds-col12a1a_e1-E1b:mCherry-Ds, Cat# 210386).

Data and code availability

Raw and processed data generated in this study were submitted to GEO (GEO: GSE178751). Custom code for an analysis pipeline of bulk ATAC-seq data, including gene regulatory network analysis, is available on GitHub (https://github.com/michaelweinberger/ATACseq_GRN_analysis, Zenodo: https://doi.org/10.5281/zenodo.10384511). Any additional information required to re-analyze the data reported in this paper is available from the lead contact upon request.

EXPERIMENTAL MODEL AND STUDY PARTICIPANT DETAILS

For this study, both females and males of transgenic and wildtype zebrafish strains were used. Animals used for breeding were between 3 and 24 months old. Zebrafish larvae that were used for experiments were raised to an age of 5 days post fertilisation (dpf). Larvae were euthanised and analysed shortly before reaching an age of 5dpf (free-feeding) during all experiments for which the experimental timepoint is stated as "5dpf" in text or Figures. Fish were kept at a 14 hours light, 10 hours dark cycle and fed four times a day. All animal experiments were performed under a Home Office Licence according to the Animals Scientific Procedures Act 1986, UK, and approved by the local ethics committee.

Zebrafish Lines

Published transgenic reporter lines used in this study were: *TgBAC(tcf21:H2B-Dendra2)*^{ox182},[71] *TgBAC(tcf21:myr-eGFP)*^{ox183}[71] and *Tg(βactin:Avi-Cerulean-RanGap)*^{ct700a}.[39]

Generation of transgenic zebrafish lines

To generate *TgBAC(tcf21:BirA-2a-mCherry)*^{ox143}, we used a BAC recombineering approach.[81] Briefly, a BirA-2A-Cherry-SV40pA-FRT-Kan-FRT cassette was PCR-amplified using Herculase II fusion DNA polymerase (Agilent Technologies) and recombined into the first coding exon of *tcf21* within the DKEYP 79F12 BAC clone as previously described.[71] In a second recombination step, an iTol2-Ampicillin cassette (provided by Prof. Kawakami, National Institute of Genetics, Mishima, Japan) was introduced into the BAC backbone as previously published.[81] Wild-type embryos were injected at the one-cell stage with 200 ng/μl of purified BAC DNA and 100 ng/μl *tol2* transposase mRNA. Putative founders were outcrossed to wild-type fish and offspring screened for Cherry expression, in combination with PCR amplification of the transgene when expression levels were low.

Tg(mdka_e1:mCherry)^{ox195}, *Tg(mdka_e2:mCherry)*^{ox197} and *Tg(col12a1a_e1:mCherry)*^{ox196} were generated by plasmid transgenesis. To generate pVC-Ds-mdka_e1-E1b:mCherry-Ds, pVC-Ds-mdka_e2-E1b:mCherry-Ds, pVC-Ds-col12a1a_e1-E1b:mCherry-Ds, genomic sequences were amplified from wildtype DNA using Herculase II fusion DNA polymerase (Agilent Technologies). Sequence coordinates in GRCz10 and primers used for amplification are listed in Table S2. eGFP was replaced with mCherry in the pVC-Ds-E1b:eGFP-Ds plasmid (#102417, Addgene).[82] The plasmid was then linearised with NheI and XhoI (NEB) and amplified sequences were inserted using InFusion (InFusion HD Cloning kit, Clontech). Wild-type embryos were injected at the one-cell stage with 30 ng/μl of purified plasmid DNA and 10 ng/μl *Ac* transposase mRNA. For all constructs, stable expression lines were generated. At 5dpf, F1 larvae were euthanized using MS222 and the heart was imaged as soon as it stopped beating. Hearts were not aligned according to their contraction cycle status. Images were obtained using a LSM780 confocal microscope (ZEISS) and a 20x objective.

METHOD DETAILS

Hybridisation Chain Reaction

Wildtype larvae were euthanised using tricaine methanesulfonate (MS-222) and fixed in 4% paraformaldehyde (PFA) overnight at 4°C. Subsequently, larvae were stored at -20°C in methanol. Hybridisation chain reaction (HCR) v3.0[44] was performed following a protocol by Choi et al. Briefly, larvae were permeabilized using 30μg/ml proteinase K for 45 minutes at room temperature, post-fixed in 4% PFA and incubated overnight at 37°C in 30% probe hybridisation buffer containing 2pmol of each probe mixture. Excess probes were washed off with 30% probe wash buffer at 37°C and 5X Sodium Chloride Sodium Citrate/0.1% Tween 20 (SSCT) at room temperature and larvae were incubated overnight at room temperature in amplification buffer containing 15pmol of each fluorescently labelled hairpin. Following HCR, larvae were incubated with Hoechst reagent (1:1000, 5XSSCT) for 30 minutes at room temperature.

Adult injured and sham-control hearts were collected and fixed in 4% paraformaldehyde (PFA) for 2h at room temperature. OCT-embedded hearts were cryosectioned and 10μm sections were then washed in DEPC-treated water and permeabilised for 10 minutes using PBS/0.1% Tween 20. Staining was performed as previously described,[44] with the following adaptations: sections were pre-hybridised with 30% probe hybridization buffer for 10 min at 37 °C in a humidified chamber. Sections were then incubated with 1.6 pmol of each DNA probe (Molecular Instruments) diluted in hybridization buffer, covered with a cover slip and incubated overnight at 37 °C in a humidified chamber. Sections were washed in 30% probe wash buffer and 5X Sodium Chloride Sodium Citrate/0.1% Tween 20 (SSCT) at room temperature and then incubated for 30 minutes at room temperature in amplification buffer. Hairpins were incubated at final concentration of 6 pmol each (amplifier B1-Alexa488, amplifier B3-Alexa594, and amplifier B4-Alexa546; Molecular Instruments), overnight at room temperature in a dark humidified chamber. Excess hairpins were washed in 5X SSCT and nuclei stained with Hoechst reagent (1:1000, 5XSSCT) for 10 minutes at room temperature.

Probe sequences were designed by the manufacturer probe (Molecular Instruments), probe sets used were: dr_tcf21 (amplifier B1), col12a1a_dr (amplifier B3), mdka_dr (amplifier B4), postnb_dr (amplifier B4), klf9_dr (amplifier B5), tbx2b_dr (amplifier B3), sox4-a_dr (amplifier B2), meis1b_dr (amplifier B5), nrf1_dr (amplifier B2), zbtb7a_dr (amplifier B5), hif1ab_dr (amplifier B4). Images were obtained using a LSM780 confocal microscope (ZEISS) using 10x and 40x objectives. Contrast and brightness were adjusted separately for each colour channel.

Immunocytochemistry

Harvested adult hearts were fixed in 4% PFA at 4°C overnight, embedded into optimal cutting temperature (OCT) compound, sectioned at 20μm thickness on a microtome-cryostat and stored at -20°C. For immunocytochemistry, sections were washed with PBS-T (PBS, 0.1% Triton) and blocked using 5% goat serum in PBS-T for 1 hour at room temperature. When staining against PCNA, heart sections were boiled in antigen retrieval buffer (H-3300, Vectorlabs) for 5 minutes in a pressure cooker before blocking. Primary antibodies used were: chicken anti-GFP (ab13970, abcam, 1:500), mouse anti-mCherry (632543, Clontech, 1:500), rabbit anti-Dendra2 (PA5-122326, ThermoFisher, 1:200), mouse IgG2b anti-MYH1E (MF20, DSHB, 1:200), mouse IgG2a anti-PCNA (ab29, abcam, 1:200) added overnight at 4°C. Secondary antibodies and Hoechst reagent were used at 1:1000 dilution and added for 2 hours at room temperature. Images were obtained using a LSM780 confocal microscope (ZEISS) and 10x, 40x objectives. Contrast and brightness were adjusted separately for each colour channel.

To analyse ventricular *tcf21*:H2B-Dendra2^{+} cell numbers outside the wound, we counted Dendra2 fluorescent cells on the parts of the ventricular surface that were located outside the injury area. We however excluded the region between bulbus arteriosus and atrium since it was hard to distinguish ventricular, bulbus or atrial Dendra2 fluorescent cells in this area.

Histology

Harvested adult hearts were fixed in 4% PFA at 4°C overnight, embedded into paraffin wax and 7μm sections deparaffinised, rehydrated and washed in distilled water. Acid Fuchsin Orange-G (AFOG) staining was performed as described previously.[4] The fibrotic tissue region (tissue stained red as well as surrounding tissue featuring blue staining) and the ventricular surface were demarcated, and areas measured using ZEN Blue software (ZEISS). The percentage of the fibrotic tissue area relative to the entire ventricle area was calculated. The thickness of the compact muscle layer for each section was measured at both ends of the fibrotic tissue area and averaged. Compact muscle was defined as non-fibrous tissue, located at the lateral edges of the fibrotic tissue area, as well as being located between the fibrotic tissue and the outer surface of the ventricle.

Larval heart Isolation, Dissociation and FAC-Sorting

Larvae were euthanised using MS-222 and larval hearts were isolated following a published protocol,[83] using a 21-gauge needle for disruption. This procedure recovered around 50% of the larval hearts. Hearts were dissociated using 15mg/ml collagenase (C8176, Sigma Aldrich) in 0.05% trypsin solution at 30°C for 14mins. 7-AAD cell viability dye was used to exclude non-viable cells during FACS. 1000-2000 fluorescent cells and 1000-2000 non-fluorescent cells were purified from *TgBAC(tcf21:H2B-Dendra2)*^{ox182} (200 hearts). Cells sorted in separate FACS sessions were processed separately during RNA-seq or ATAC-seq library preparation.

Adult mCherry^{+} epicardial cells were FACS-isolated from *TgBAC(tcf21:BirA-Cherry)*^{ox143} operated adult hearts (1 heart per biological sample). Prior to FACS, heart tissue was dissociated using 20 mg/ml collagenase in 0.05% Trypsin/0.53 mM EDTA/1xHBSS buffer to obtain single cell suspensions. Reaction was stopped in 10 mM HEPES/0.25% BSA/1xHBSS buffer and mCherry^{+} cells were sorted (FACSAria, BD Biosciences Fusion System). 300-500 fluorescent cells were purified from each *TgBAC(tcf21:BirA-Cherry)*^{ox143} heart. Cells sorted in separate FACS sessions were processed separately during ATAC-seq library preparation.

Adult zebrafish heart injury

Cardiac injuries were carried out in 4–12 month old zebrafish.[3,5] Briefly, cryoinjury was performed by application of a cryoprobe frozen with liquid nitrogen to the surface of the exposed ventricle until the probe was fully thawed, damaging approximately 20% of the ventricle. Exposing the ventricle, without injury, was performed for sham controls. Cryoinjured and sham-control hearts were harvested 3, 7 and 22 days after injury/sham (dpi and dps, respectively).

Biotagged nuclei isolation

Biotagged nuclei were isolated as previously described.[38,39] Briefly, *TgBAC(tcf21:BirA-Cherry)*^{ox143}*; Tg(βactin:Avi-Cerulean-RanGap)*^{ct700a} operated adult hearts (n = 2 per sample) were washed and incubated on ice in hypotonic buffer H (20 mM HEPES, pH 7.9; 15 mM MgCl2; 10 mM KCl; 1 mM DTT; 1 X Complete protease inhibitor) for 30 min. Heart samples were transferred to a Dounce homogenizer (2 ml Kontes Glass Co, Vineland, NJ) and dissociated by 10 strokes with the loose fitting pestle A and incubated on ice for 5 min. Further dissociation was carried out by 10 strokes with tight fitting pestle B, performed every 5 min for 15 min. Nuclei were collected by centrifugation (2000 × g, 4 °C) and re-suspended in 1 ml of nuclei pulldown buffer NPB buffer (10 mM HEPES, pH 7.9; 40 mM NaCl; 90 mM KCl; 0.5 mM EDTA; 0.5 mM spermidine; 0.15 mM spermine; 1 mM dithiothreitol and 1 X Complete protease inhibitor). For nuclei purification, nuclei were incubated with 250 μg of M-280 streptavidin-coated dynabeads (Invitrogen) with rotation for 30 min at 4 °C. A flow-based system was used to capture the nuclei bound on the streptavidin beads. A 10 ml seriological pipette (VWR) attached to a 1 ml micropipette tip (Rainin reach pipet tip), both pre-treated with NPB+1% BSA for 30 min, was added to a MiniMACS separator magnet (OctoMACS Separator, Miltenyl Biotec). A two-way stopcock (Biorad) was connected to the end of the 1 ml micropipette tip via a piece of Tygon tubing (Fisher Scientific) and the flow-rate set to ~0.75 ml/min. The nuclei beads suspension was diluted by addition of 9 ml of NPBt (NPB with 0.01% Triton X-100) and added to the slow-flow setup. The tip was subsequently removed from the stand and the nuclei-beads released from the tip by slowly pipetting 1 ml of NPBt in and out of the tip. The solution was then diluted again to 10 ml with NPBt and added again to the slow-flow setup. Nuclei-beads were eluted in 1 ml of NPBt as described above and the NPBt removed using a magnetic stand (DynaMag TM-2 magnet, Invitrogen). Nuclei-beads were then processed for RNA extraction.

RNA extraction and library preparation for sequencing

1000 FACS-purified cells from *TgBAC(tcf21:H2B-Dendra2)*^{ox182} larvae were processed using the SMART-SeqTm v4 UltraTm Low Input RNA Kit for Sequencing (Takara Clontech). Samples were lysed and poly-adenylated RNA reverse transcribed via SMARTScribe Reverse Transcriptase. Following reverse transcription, cDNA was amplified with SeqAmp DNA Polymerase, using 11 PCR cycles. Amplified cDNA was purified using Agencourt AMPure XP beads (Beckman Coulter). The purified cDNA was quantified using Qubit Fluorometric Quantitation (ThermoFisher) and the quality was verified on an Agilent 2100 Bioanalyzer (Agilent Technologies). Final sequencing libraries were prepared using the Nextera XT DNA Library Preparation Kit (Illumina). 1ng cDNA was used as input, samples were tagmented for 5 minutes and 10 seconds and amplified using 12 PCR cycles. The libraries were quantified using Qubit Fluorometric Quantitation (ThermoFisher) and their quality checked on a 2200 TapeStation system (Agilent). All cDNA libraries were pooled and sequenced to a depth of 355 million reads on a NextSeq500 machine (Illumina, 150 Cycle High Output Kit).

Total nuclear RNA extraction and DNase treatment of *TgBAC(tcf21:BirA-Cherry)*^{ox143}*; Tg(βactin:Avi-Cerulean-RanGap)*^{ct700a} adult-derived epicardial nuclei (1000–2000 nuclei per biological sample) were carried out using the RNAqueous Micro Kit (Life Technologies) according to manufacturer's instructions. RNA integrity was checked with an RNA pico chip (Agilent Technologies) using the Agilent 2100 Bioanalyzer (Agilent Technologies). cDNA was synthesized and amplified from 100 pg–300 pg of input RNA using SMART-seqTMv4 Ultra Low input RNA kit (Takara Clontech). Sequencing libraries were prepared using the Nextera XT DNA library preparation kit (Illumina). Next Generation Sequencing was performed on a NextSeq500 platform using a NextSeqTM500 150-cycle High Output Kit) (Illumina) to generate 80-basepair paired end reads.

ATAC Sequencing

ATAC-seq was performed following a protocol modified from Buenrostro and colleagues.[29] FACS purified cells from *TgBAC(tcf21:H2B-Dendra2)*^{ox182} larvae were pelleted at 600g for 7.5 minutes at 4°C, washed, pelleted, lysed and pelleted at 600g for 10 minutes at 4°C. Samples were then tagmented using 0.25μl Tn5 in 5μl TD buffer and 4.75μl H_2O for 30 minutes at 37°C. Then, EDTA was added to a concentration of 50mM and samples were incubated for 30 minutes at 50°C. $MgCl_2$ was added to a concentration of 50mM and 16μl of each sample were PCR amplified using 2x NEB Next HiFi PCR mix (NEB) and 16 PCR cycles.

FACS purified cells from *TgBAC(tcf21:BirA-2a-mCherry)*^{ox143} adult hearts were pelleted at 500g for 5 minutes at 4°C, washed with ice cold 1X PBS buffer and pelleted again 500g for 5 minutes at 4°C. Cells were then lysed by gentle resuspension in cold lysis buffer (10 mMTris-HCl, pH 7.4; 10 mM NaCl; 3 mM $MgCl_2$; 0.1% IGEPAL CA-630) and immediately spun down at 500xg for 10 minutes at 4°C. Samples were then tagmented using 0.25μl Tn5 in 5μl TD buffer and 4.75μl H_2O for 20 minutes at 37°C. Samples were quenched by adding EDTA to a concentration of 50mM and incubated for 30 minutes at 50°C. MgCl2 was added to a final concentration of 50mM and 12.2μl of each tagmented sample was PCR amplified for 15 cycles using 2x NEB Next HiFi PCR mix (NEB). Amplified libraries were purified using the Qiagen PCR purification MinElute kit.

The quality of the ATAC libraries was checked on a 2200 TapeStation system (Agilent). Libraries were sequenced to a depth of approximately 50 million reads per sample (Illumina, 75 Cycle High Output Kits).

Electroporation of enhancer reporter constructs into the adult zebrafish heart

Anesthetised adult zebrafish were kept with their ventral side facing upwards, immobilised in a damp sponge. For reporter constructs, 2μg of the plasmid of interest (4μl of a 0.5μg/μl injection solution) were injected into the pericardial cavity using a 30G insulin syringe after exposing the ventricle. For gene editing experiments, 400ng of a *ubb*:Cas9 plasmid containing Tol2 recognition sites,[51] 40ng of a *CMV*:Tol2 plasmid (both plasmids provided by Richard White) and 8000ng sgRNA mix (1000ng per *hif1ab*, *nrf1*, *tbx2b*, *zbtb7a* sgRNA, 2 sgRNAs per gene) were injected into the pericardial cavity in a 2.4μl volume. In the control condition, the transcription factor sgRNA mix was replaced with 8000ng of a sgRNA targeting *AmCyan*. For the gene editing test experiment, 400ng *ubb*:-Cas9, 40ng *CMV*:Tol2 and 2000ng of a sgRNA targeting *eGFP* or 1000ng of *AmCyan* sgRNA were injected in a 1μl volume. *AmCyan* and *eGFP* sgRNAs have been described previously,[71] all sgRNAs were ordered as Alt-R™ HDR Donor Oligos (IDT, sgRNA sequences listed in Table S3). Electrodes (Genepaddles, 3×5 mm) were placed on either side of the heart cavity and electric current was applied in a set up with voltage of 35V, 5 pulses, 100ms pulse length and 50ms pulse interval. To maximise DNA entering the epicardial layer, which is located at the surface of the heart, the cathode and the anode location was swapped after electroporation and electric current was applied once more. Zebrafish were immediately returned to fresh water after electroporation.

QUANTIFICATION AND STATISTICAL ANALYSIS

Statistical details of experiments can be found in the Figure legends, including p-values and numbers of samples analysed. Unless noted otherwise, adjusted p-values of below 0.05 were treated as significant. Plots were generated with ggplot2[84] in R. Some plots include box and whiskers plots (in the style of Tukey), indicating median and first/third quartiles.

Published Datasets

Previously published transcriptomic data[55] was used to analyse TF expression in the uninjured adult zebrafish epicardium (GEO: GSE172511).

RNA Sequencing Data Analysis

Transcriptomic data was mapped to the zebrafish reference genome (GRCz10-91) using the STAR gapped aligner.[72] Duplicate reads were removed with samtools (v1.10)[74] and reads were summarized on gene level (including both protein-coding and non-coding genes) using featureCounts.[75] Differential gene expression analysis and principal component analysis were performed in R (v4.0.3) using DESeq2 (v1.30.0).[76] Counts were transformed into FPKM expression values with the rpkm() command in the edgeR package (v3.32.1)[77] and heatmaps drawn using pheatmap (v1.0.12). Gene ontology term analysis was performed with the topGO package (v2.42.0),[78] using differentially expressed genes with an adjusted p-value below 0.001.

ATAC Sequencing Data Analysis

Sequencing reads were mapped to the zebrafish reference genome (GRCz10-91) using the bowtie aligner (v1.2.3).[73] Duplicate reads were removed with samtools (v1.10). BAM files were converted to bigWig format and accessibility tracks were visualised in the UCSC Genome Browser. BAM files were converted to BED format and peaks were called using MACS (v2.2.7.1, callpeak -B -f BED -g 1.37e09 –call-summits).[45] The Homer (v20201202)[47] script ''annotatePeaks.pl'' was used to annotate peaks to the closest expressed gene in each condition and to genomic features, to do TSS enrichment analysis and to compute CpG and GC content. For this, fasta and gtf files for GRCz10 were obtained from the UCSC Genome Browser[85] website. The R package DiffBind (v3.0.13)[46] was then used to construct a consensus peak set across all samples, removing peaks contained in less than two samples and peaks overlapping repetitive elements in the genome, and resizing all peak widths to 500bp. Peak names were assigned based on genomic position as P.*[chromosome].[start position]*. Peak accessibility FPKM values were computed manually. DESeq2 (v1.30.0) was used for differential peak accessibility analysis. Gene ontology term analysis was performed with the R package topGO (v2.42.0), using genes that differentially accessible peaks with an adjusted p-value below 0.05 and a baseMean above 20 were annotated to.

Transcription Factor Binding Site Analysis

For analysis of TF binding in identified peak regions, TF motifs were identified across the consensus peak set, as well as in the putative enhancer sequences used for the *in vivo* enhancer activity assay, using the ''gimmescan'' command in the gimmemotifs package[79] and the JASPAR2020 (v0.99.10) core vertebrates transcription factor motif database.[52] A false positive rate of 0.05 (-f 0.05) was used as a cutoff when calling motifs across the consensus peak set. When calling motifs in the enhancer sequences, a cutoff score of 0.6 (-c 0.6) was used and motifs with a score below 8.9 were subsequently excluded. Motifs belonging to TFs with a centrality of <0.25 in the relevant network were also excluded. The R chromVAR (v1.12.0) package[53] was used cluster samples according to TF motif accessibility and to plot motif logos.

Gene Regulatory Networks

Gene regulatory networks were constructed using the Python package Ananse (v0.1.7).[59] To construct the *tcf21* larval network, input was extracted from *tcf21* larval ATAC-seq and RNA-seq samples, *tcf21* cryo samples were used for the *tcf21* cryo network and *tcf21* sham samples for the *tcf21* sham network. As ATAC-seq input, a consensus peak set across samples of the relevant condition was constructed using DiffBind, and the mean FPKM accessibility values were computed. As RNA-seq input, mean TPM gene expression values were computed manually. Additionally, gene positions were extracted from the GRCz10 GTF file and stored in BED format. The JASPAR2020 (v0.99.10) core vertebrates transcription factor motif database[52] was used to acquire TF binding motifs. ''prob'' values in the Ananse network output (termed ''network scores'' in Figure 6) were taken forward to indicate the strength of connections in the network. Ananse networks were subset to only contain connections with a strength above 0.99. The sub-networks were transformed into weighted directed graphs (''prob'' values were used as weights) and the eigenvector centrality (evcent) computed using R igraph (v1.2.6). The in-degree centrality was computed via: degree(g, mode = "in") / (vcount(g) - 1), following a previous approach.[86] Network graph schematics were plotted using BioTapestry (v7.1.2.0),[80] using network connections between the indicated TFs with a strength above 0.995.